International Journal of Heat and Mass Transfer 196 (2022) 123291

Contents lists available at ScienceDirect

International Journal of Heat and Mass Transfer

journal homepage: www.elsevier.com/locate/hmt

Assessment and development of flow boiling critical heat flux correlations for partially heated rectangular channels in different gravitational environments

Steven J. Darges, V.S. Devahdhanush, Issam Mudawar*

Purdue University Boiling and Two-Phase Flow Laboratory (PU-BTPFL), School of Mechanical Engineering, Purdue University, 585 Purdue Mall, West Lafayette, IN 47907, USA

ARTICLE INFO

Article history:
Received 23 March 2022
Revised 19 June 2022
Accepted 24 July 2022
Available online 4 August 2022

Keywords:
Critical heat flux
Flow boiling
Partial heating
Design correlation
Gravitational effects

ABSTRACT

This study investigates critical heat flux (CHF) of n-Perfluorohexane flowing in a partially heated rectangular channel of 2.5-mm × 5.0-mm cross-section, within NASA's Flow Boiling and Condensation Experiment's (FBCE) Flow Boiling Module (FBM). A consolidated FBCE-CHF database is formed by compiling datasets from prior years of testing the FBM both at different orientations in Earth gravity (horizontal flow, vertical upflow, and vertical downflow) and on parabolic flights until it was launched to the International Space Station (ISS) in August 2021. This database encompasses a wide range of operating conditions (both subcooled liquid inlet of different inlet subcoolings and saturated two-phase inlet of different inlet qualities at different mass velocities and system pressures), heating configurations (single- and double-sided inlet), and different gravitational environments. The database is further categorized into three based on the type of CHF: subcooled CHF, saturated CHF with single-phase inlet, and saturated CHF with two-phase inlet. An exhaustive literature search is conducted to identify almost all flow boiling CHF correlations, which are then utilized to make predictions of the database and their accuracies assessed for each small subset of the database. Some correlations are capable of providing adequate CHF predictions for large portions of the database, while some provide very good predictions for very small subsets of operating conditions, typically those for which they were developed for. No single existing correlation is capable of predicting the entire database with good accuracy. Many correlations do not consider the effects of gravity on CHF, which is important for the different orientations tested, and even the few that do, are unsuccessful in predicting the microgravity data. A new simple CHF correlation is developed to address the drawbacks of the existing ones and is easy to use. This new correlation predicts the entire consolidated database with a mean absolute error of 17.44% with good accuracies for each subset of the database.

1. Introduction

1.1. Two-phase thermal management systems

Adequate heat dissipation is crucial for dependable and safe operation of many modern devices. Conventionally, single-phase thermal management systems, through either air or liquid cooling, have been the standard for thermal management. However, as heat dissipation requirements increase, single-phase systems are no longer able to meet the necessary cooling demands. To combat the considerable heat dissipation requirements of high heat flux devices used in computing, medical, transportation, energy, aerospace, and defense applications [1], two-phase thermal management systems, which take advantage of both the coolant's sensible and latent heat, can be adopted to ensure sufficient cooling and maintain the devices at safe temperature. Not only are two-phase thermal management systems capable of handling larger heat loads than their single-phase counterparts, but they also achieve this with lighter, more compact systems, which is an important design aspect especially in the aerospace industry.

Thermal engineers optimize the configuration of two-phase thermal management systems in order to realize their full potential for any given application. This greatly depends on the cooling requirements, size and weight constraints, available power supply, and operational environment of the system. The Purdue University Boiling and Two-Phase Flow Laboratory (PU-BTPFL) has made

* Corresponding author.
E-mail address: mudawar@ecn.purdue.edu (I. Mudawar).
URL: https://engineering.purdue.edu/BTPFL

https://doi.org/10.1016/j.ijheatmasstransfer.2022.123291
0017-9310/

Nomenclature

A	area; channel cross-sectional area
Bd	Bond number, $g(\rho_f - \rho_g)D^2/\sigma$
Bd_θ	orientation-specific Bond number, $g\cos\theta(\rho_f - \rho_g)D^2/\sigma$
Bi	Biot number, hL/k
Bo_{CHF}	boiling number at CHF, $q''_{CHF}/(Gh_{fg})$
C	constant
Ca	capillary number, $G\mu_f/(\rho_f\sigma)$
Co	confinement number, $\sqrt{\sigma/g(\rho_f - \rho_g)}/D$
c_p	specific heat at constant pressure
D	diameter
D_e	equivalent heated diameter, $4A/P_h$
D_h	hydraulic diameter
Fr	Froude number, $G^2/(\rho_f^2 gD)$
Fr_θ	orientation-specific Froude number, $G^2/(\rho_f^2 g\sin\theta D)$
G	mass velocity
g	gravitational acceleration
g_e	gravitational acceleration on Earth
μg	microgravity
H	longer dimension of channel's cross-section
h	enthalpy
h_{fg}	latent heat of vaporization
k	thermal conductivity
L	length
$\dot{m}$	mass flow rate
N	number of datapoints
P	perimeter
p	pressure
p_r	reduced pressure
q''	heat flux
q''_{CHF}	critical heat flux
Re	Reynolds number, GD/μ_f
T	temperature
ΔT_{sub}	fluid subcooling, $T_{sat} - T_f$
U	mean channel velocity
u	velocity
W	shorter dimension (width) of channel's cross-section
We	Weber number
We_D	Weber number based on channel diameter, $G^2D/(\rho_f\sigma)$
We_L	Weber number based on channel heated length, $G^2L_h/(\rho_f\sigma)$
x_e	thermodynamic equilibrium quality
Y	Shah's correlating parameter, $Y = \left(\frac{GDc_{p,f}}{k_f}\right)\left(\frac{G^2}{\rho_f^2 gD}\right)^{0.4}\left(\frac{\mu_f}{\mu_g}\right)^{0.6}$

Greek symbols

α	void fraction
β	aspect ratio, H/W
θ	orientation angle of channel
μ	dynamic viscosity
ξ_{30}	percentage of datapoints predicted within ±30%
ξ_{50}	percentage of datapoints predicted within ±50%
ρ	density
σ	surface tension

Subscripts

CHF	corresponding to critical heat flux
De	calculated using $D = D_e$
exp	experimental
f	saturated liquid
g	saturated vapor
h	heated
in	channel heated section inlet; inlet
out	channel heated section outlet; outlet
$pred$	predicted
s	solid
sat	saturation
w	wetted

Acronyms

BHM	Bulk Heater Module
CHF	Critical Heat Flux
FBCE	Flow Boiling and Condensation Experiment
FBM	Flow Boiling Module
ISS	International Space Station
MAE	Mean Absolute Error (%)
MST	Mission Sequence Testing
RMSE	Root Mean Square Error (%)

it a priority to provide valuable information regarding the design and performance of numerous two-phase cooling schemes including capillary flow [2], pool boiling [3], falling films [4], flow boiling in macro-channels [5,6], micro-channels [6–8], and annuli [9], spray cooling [10], jet impingement cooling [11,12], and hybrids between different configurations [13]. Each scheme possesses its own advantages and disadvantages, that merit implementation in unique situations. The present study is focused on channel flow boiling, whose benefits include a simple flow loop requiring relatively low pumping power, flow inertia aiding in vapor removal from heated surfaces, and the potential to cool multiple devices in series in a fully closed loop.

1.2. Critical heat flux

Arguably the most important design parameter to consider for a heat-flux-controlled boiling system is critical heat flux (CHF). CHF marks the transition between the nucleate boiling and film boiling regimes, which have drastically different characteristics and performance. Operation in the nucleate boiling regime is associated with relatively low degrees of wall superheat and high heat transfer coefficients, prompting efficient heat transfer. This is due to the mechanism of heat transfer predominantly being bubble nucleation and the prediodic replenishment of liquid at the heated wall. Once vapor prevents liquid from accessing the heated wall, a commonly recognized trigger mechanism for CHF, the film boiling regime is entered. Heat from the heated wall is dissipated as conduction through the vapor film to the liquid-vapor interface where evaporation occurs. Due to the dreadfully low thermal conductivity of vapor, wall temperatures escalate, and heat transfer coefficients plummet, making it inferior to the nucleate boiling regime. This transition usually causes device damage and system failure.

CHF is classically segregated by quality at the downstream location of CHF into either subcooled, $x_{e,CHF} < 0$ or saturated, $x_{e,CHF} \geq 0$. The aforementioned abrupt transition from the nucleate to film boiling regime is described as departure from nucleate boiling (DNB). It occurs with either subcooled CHF or low-quality saturated CHF where, as the name suggests, nucleate boiling suddenly comes to a halt. However, this is not the sole mechanism of CHF. Dryout is another prevalent CHF mechanism and occurs as a relatively tame transition of flow regimes along the length of the channel from bubbly to slug, to annular, and eventually to mist at the downstream portion of the heated length, where dryout occurs. It is predominantly associated with saturated inlet conditions, thus

saturated CHF, and is identified by the annular flow regime occupying a large portion of the channel and the gradual thinning of the liquid film. Dryout incipience precedes dryout and acts as an indicator or nearing CHF. At this point, local dry patches form and degradation of heat transfer coefficients begin but rewetting of the wall prevents CHF. Once dryout completion occurs, the outlet portion of the channel is occupied entirely by the mist regime, which does not sufficiently cool the wall. This culminates in a steady rise in wall temperatures that eventually leads to CHF.

1.3. CHF prediction methods

Due to the potentially catastrophic effects of CHF, it is imperative reliable predictive tools are available to aid in designing systems to safely operate in the nucleate boiling regime. The most robust prediction methods are analytical models derived from flow physics. However, few models exist such as *Boundary Layer Separation* [14], *Bubble Crowding* [15], *Sublayer Dryout* [16], and *Interfacial Lift-off* [17]. These analytical models generally have broad applicability with the prerequisite of presence of the physical phenomena the model describes. While the value of analytical models should not be understated due to their physical formulation, their complexity can be unappealing. Simple correlations that are continuous functions of few dimensionless numbers are desirable when running simulations of thermo-hydraulic systems using fast numerical codes [18]. Because of this, empirical correlations are the most common approach to predict CHF; however, they have inherent shortcomings because they are developed for specific geometries and operating conditions. One common criterion for a correlation is its applicability for either subcooled or saturated CHF. Extrapolating correlations to previously untested operating conditions is risky and can result in large errors [19,20].

In the past 70 years, an abundance of flow boiling CHF correlations have been proposed with many of the earliest correlations exclusively developed for nuclear reactors [21–25]. This is reflected in the narrow scope of operating ranges recommended for the correlation, typically highly pressurized, subcooled water. However, these primitive CHF correlations determined a befitting functional form of $q''_{CHF} = f(L, D, G, p, \Delta T_{sub})$, which has remained in many contemporary correlations for a wider variety of applications, and thus vastly different operating conditions than those in nuclear reactors. Recognizing the bias towards high pressure operating conditions, Celata *et al.* [26] used a database of water compiled from numerous sources to modify Tong's correlation [27], which was derived from the boundary layer separation analysis of Kutateladze [14]. Maintaining the same functional form, Celata *et al.* tweaked the method of determining the coefficient to predict q''_{CHF} at lower pressures. Vandervort *et al.* [28] aimed to correlate flow boiling CHF of water in the high flux region defined as $q''_{CHF} = 10^7 - 2\times10^8$ W/m^2. They took a statistical approach to develop a correlation featuring a large number of constants, which were then adjusted to eliminate non-physical predictions at the lower extremes of operating ranges. Hall and Mudawar [19] amassed a comprehensive database for subcooled CHF of water in uniformly heated tubes. Analyzing parametric trends within a subset of the database, they developed dimensionless correlations that proved accurate for the entire database. They identified two acceptable forms for a correlation [20], one based on inlet conditions, $q''_{CHF} = f(L, D, G, p, h_{in})$, and the other on outlet conditions, $q''_{CHF} = f(D, G, p, h_{out})$, matching crucial variables determined by the earliest correlations. Zhang *et al.* [29] also compiled a database for flow boiling CHF of water in uniformly heated tubes, albeit smaller than the database by Hall and Mudawar, but including saturated CHF data. They concluded the correlation by Hall and Mudawar was sufficient for predicting subcooled CHF and proposed a new dimensionless correlation for saturated CHF.

The plentiful availability of water data has led to the development of many correlations specializing in CHF predictions for water. However, applications requiring fluids other than water require correlations that have also been verified for those fluids. One of the most widely used correlations for forced convective flow boiling in uniformly heated tubes was proposed by Katto and Ohno [30], by incorporating improvements and simplifications to a previous version by Katto [31–33]. The robustness of the correlation is shown in its broad applicability and validation for 15 different fluids. The correlation demarcates CHF into two regimes based on a density ratio of $\rho_g/\rho_f = 0.15$. In each regime, CHF is correlated with appropriate dimensionless groups and empirical constants. Similarly, Shah [34] developed a general CHF correlation for vertical upflow in uniformly heated tubes, which is applicable to 23 fluids and a wide scope of operating conditions. This correlation is based on Shah's correlating parameter, *Y*, which is a function of Peclet number, Froude number, and liquid-to-vapor viscosity ratio. *Y* was found to be significant in a previous version of the correlation [35] by analyzing parametric trends of q''_{CHF} for different working fluids. The entire correlation is divided into two subcorrelations: an upstream condition correlation (UCC) and a local condition correlation (LCC), which, as the names suggest, depends on the inlet and local conditions, respectively. Shah later expanded q''_{CHF} predictions to horizontal flow by inclusion of an additional term containing Froude number to convert predictions for vertical upflow to horizontal flow [36]. While applicable to any vertical upflow CHF correlation, Shah recommends the use of improved general correlation [34] for vertical upflow, as the multiplier was originally formulated with it. Ong and Thome [37] presented a correlation for flow boiling CHF of refrigerants in micro-channels by modifying a correlation proposed by Wojtan *et al.* [38] and included terms to account for macro-to-microscale confinement effects and viscous interfacial shear.

1.4. Gravitational effects on boiling systems

Flow boiling has been thoroughly investigated in Earth gravity, and a plethora of information is available regarding its characteristics and performance. However, presently available tools cannot necessarily be extrapolated to predict performance in an environment subject to gravities different than Earth's. The difference in body force alters the behavior of a boiling flow, rendering predictive tools that were developed in Earth gravity unreliable.

With goals of expanding the scope of space exploration missions, two-phase thermal management systems are poised to play a major role [39], making their performance in microgravity of particular interest. To improve our understanding of how phase change systems will perform in the absence of body force, researchers have pursued a variety of methods to quantify how gravity, or the lack thereof, will impact a boiling flow. The attempts to capture the influence of gravity varies in range of complexity and include experiments at different orientations in Earth gravity [40–42], using drop towers [43,44] and during parabolic flights [45,46]. During these experiments, authors have showed clear differences exist between the physics of flow boiling in microgravity and ordinary terrestrial gravity.

A review article by Konishi and Mudawar [47] of published experiments and predictive methods for boiling in microgravity identified a severe lack of predictive tools applicative to microgravity environments. They also implored researchers to focus microgravity experiments on inertia-dominated conditions where gravity has a reduced role on performance, and results will be transferable to other gravity environments. Zhang *et al.* [48] presented criteria for gravity independent flow boiling CHF by utilizing dimensionless groups that encompass key parameters and dictate flow physics. The criteria were derived from physical models describing instabil-

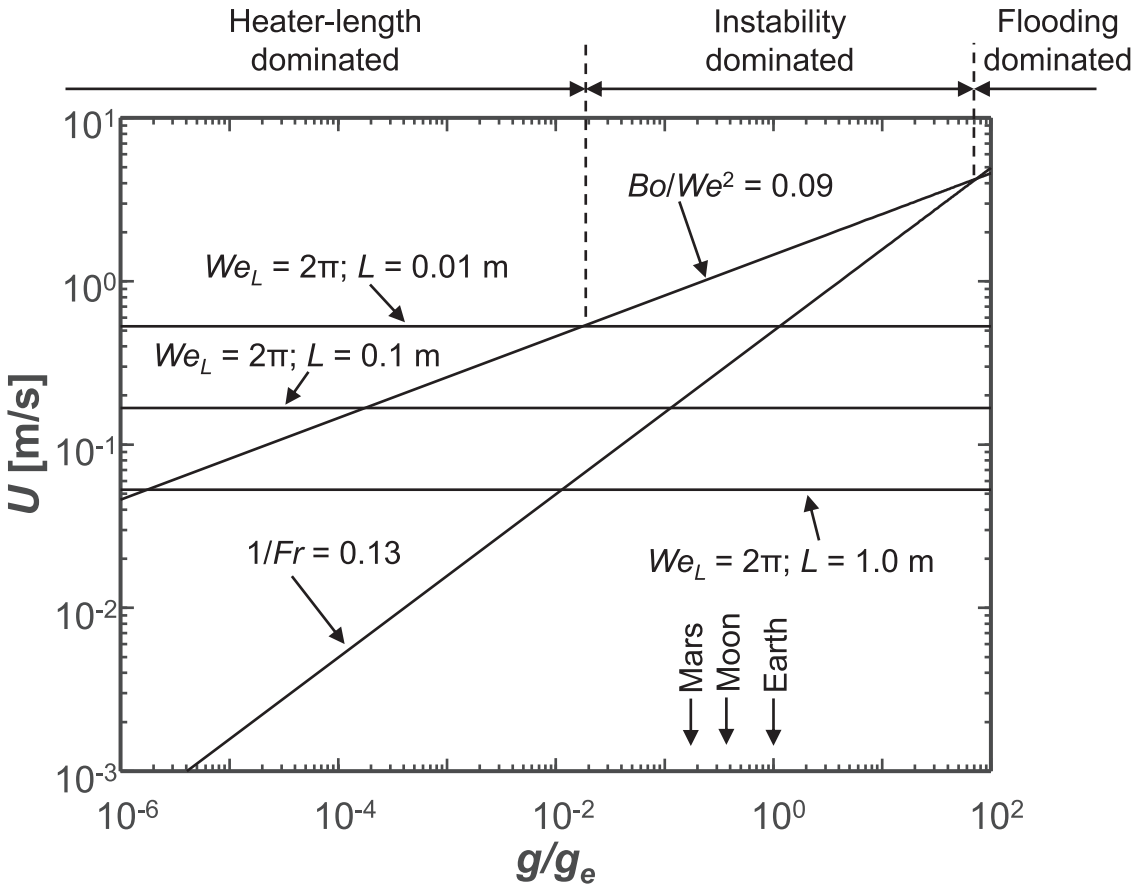

Fig. 1. Determination of minimum flow velocity required to overcome all body force effect on flow boiling CHF. Adapted from [48].

ity between a liquid vapor interface, the rising velocity of a slug bubble, which account for the components of gravity perpendicular and parallel to the heated wall, respectively. Fig. 1 displays a map that identifies regimes in which body-force-independent CHF can be achieved at different magnitudes of gravity. Note that the map contains a third region where the limiting criteria of CHF is the critical wavelength exceeding the length of heated wall with no liquid contact. This third region is derived from the instability analysis used to determine gravity independence perpendicular to the heated wall. This template was also used to provide similar criteria for gravity independent results for both flow boiling CHF with two-phase inlet [49] and condensation [50].

1.5. Partial heating

Both the geometry and heating configuration of channel restrict the use of correlations to those developed for a like, if not exact, arrangement. However, equivalent diameters can be used to expand the applicability of correlations. Classically, hydraulic diameter has been used to normalize the diameter of unique geometries to circular cross-sections. Cheng *et al.* [51] took a different approach and proposed an equivalent diameter, defined as $\sqrt{4A/\pi}$ that results in equal mass velocities and mean phase velocities, which is not achieved by the hydraulic diameter. The present study involves a rectangular channel that is heated on one side or two opposite sides. The previously mentioned diameters lack information regarding the heated portion of channel and are not capable of differentiating between the two heating configurations. Katto [52] used a heated equivalent diameter which follows the form of hydraulic diameter but heated perimeter was used instead of wetted perimeter; a similar proposal was made by Liu and Winterton [53] for flow boiling heat transer coefficient in tubes and annuli. Lee and Mudawar [54] took this a step further and used a diameter to capture not only the heated perimeter, but aspect ratio and the configuration of the heated and nonheated walls. For their parallel micro-channel heat sink, they used Shah and London's [55] expression to equate the single-phase heat transfer coefficient for rectangular channel heated on three sides to the single-phase heat transfer coefficient in a uniformly heated channel. Kureta and Akimoto [56] proposed a CHF correlation based on hydraulic diameter and included the dimensionless ratio of heated-to-wetted perimeter to account for partial heating.

1.6. Objectives of present study

The present study is part of PU-BTPFL and NASA Glenn Research Center's collaborative Flow Boiling and Condensation Experiment (FBCE), that will collect invaluable flow boiling and condensation data in microgravity on the International Space Station (ISS). This study aims to consolidate the available CHF database acquired during advancement of FBCE, which encompass a vast range of inlet qualities, multiple orientations, single- and double-sided heating configurations, as well as Earth gravity and microgravity. The database is used to assess the accuracy of numerous existing CHF correlations. A new simple correlation is developed to accurately predict q''_{CHF} for the entire database.

2. Experimental Methods

During the maturation of FBCE, modifications were made to the flow loop to ensure safe, accurate, and efficient operation of both the flow boiling module (FBM) and the components of flow loop,

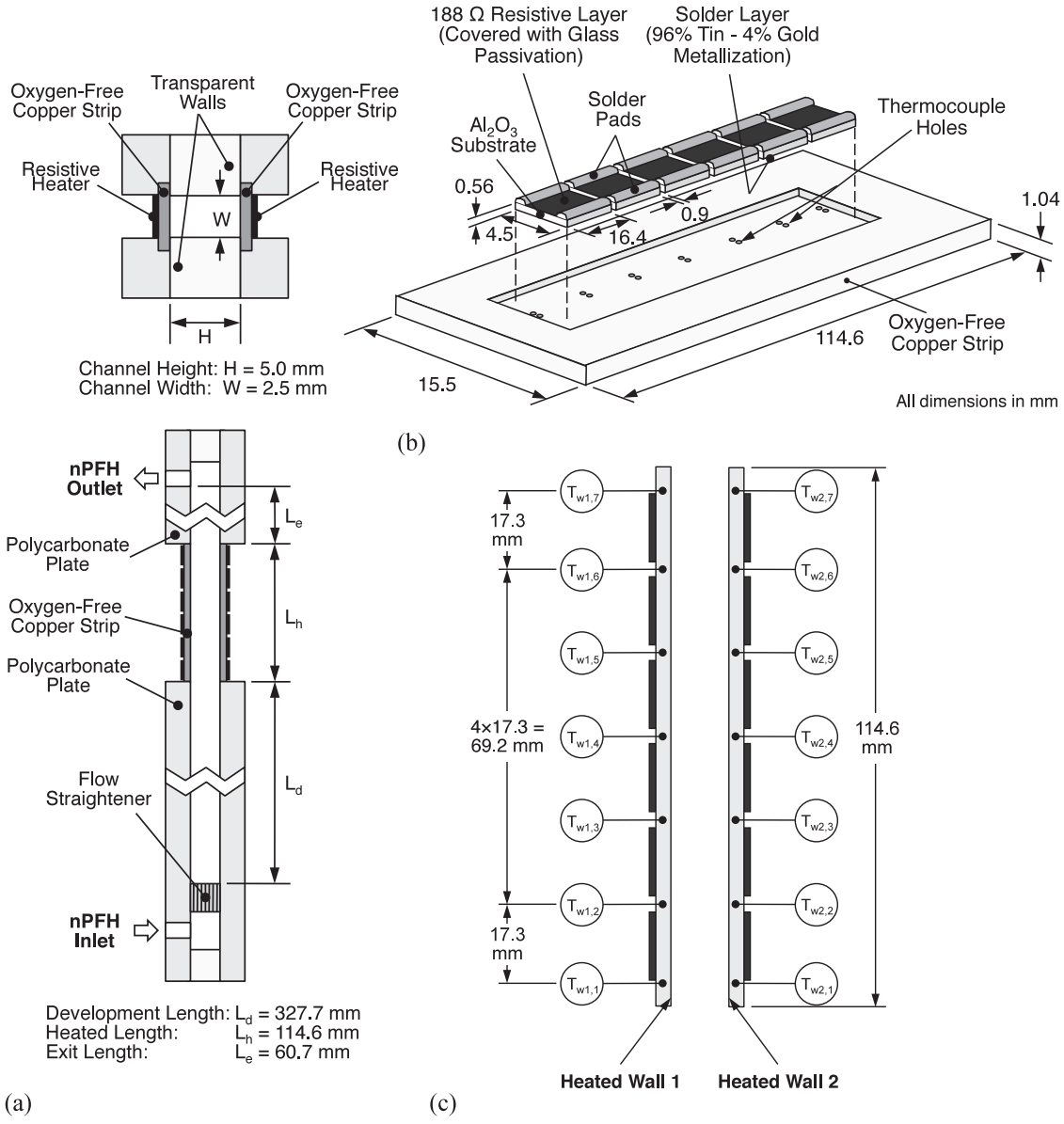

Fig. 2. Schematic representations of (a) Flow Boiling Module (FBM), (b) placement of resistive heaters on the backside of copper strip (c) location of strip thermocouples.

with the most recent iteration primed for operation on the ISS. The present study uses a consolidated database of CHF data compiled from datasets from prior years and hence minor differences in flow loop components and instrumentation exist between datasets. In this section, a brief overview of both the FBM and the most recent version of the flow loop (that has been deployed to the ISS) will be given, while also highlighting the aforementioned variations in the flow loop. For further details regarding the components, instrumentation, uncertainties, and operation of the flow loop for each dataset, readers are encouraged to reference the original publications for parabolic flight data [46], ground test data in 2014 [57,58] 2015 [42], and 2016 [59] and Mission Sequence Testing (MST, the last set of ground tests prior to deployment to the ISS) data [60–62].

2.1. Flow boiling module

A schematic diagram of the FBM, representing the test section used in all datasets, is presented in Fig. 2(a). The FBM is constructed from three transparent polycarbonate plates bolted between two aluminum support plates. A 5.0-mm deep and 2.5-mm wide rectangular slot is milled into the middle polycarbonate plate to create the flow channel. The flow channel consists of a 327.7-mm developing length, containing a honeycomb flow straightener to break up large eddies, a 114.6-mm heated length, and a 60.7-mm exit length. The heated length has 114.6-mm long, 15.5-mm wide, and 1.04-mm thick oxygen-free copper strips inserted into both the top and bottom polycarbonate plates, flush with the middle plate. Fig. 2(b) shows the placement of 6 thick-film resistive heaters of dimensions 16.4-mm length, 4.5-mm width, and 0.56-mm thickness, and a resistance of 188 Ω soldered to each of the copper strips in series, on the other side of the channel. While the copper strips are physically arranged in series, they are electrically configured in parallel to ensure uniform heating. A 0.9-mm gap between successive heater permits placement of substrate thermocouples, depicted in Fig. 2(c). The design of the heated wall has demonstrated fast temperature response time and accurate q''_{CHF} measurement [45]. All solid-solid interfaces within the FBM are made leak-proof by using NBR, HNBR, and neoprene O-rings.

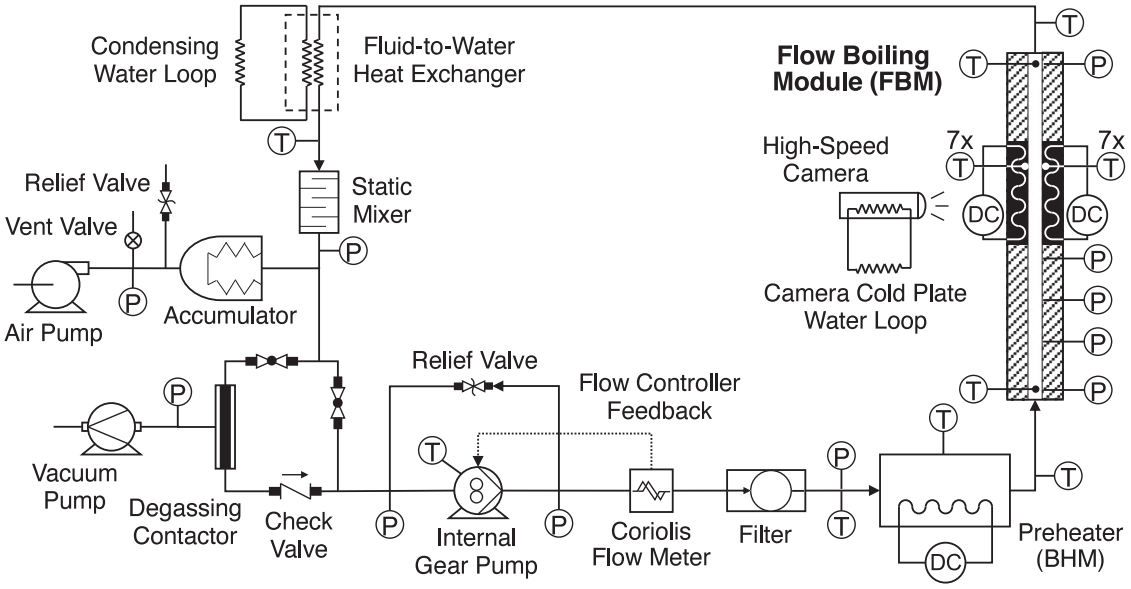

Fig. 3. Schematic diagram of two-phase flow loop used for MST.

2.2. Flow loop

The current version of the flow loop used to condition the working fluid pure normal-Perfluorohexane (nPFH, previous datasets used commercial FC-72), which is chosen for its excellent potential for themal management systems in space applications [63], is shown in Fig. 3. First, a magnetically-coupled gear pump circulates the fluid through the system. The fluid next passes through a Coriolis flow meter, where flow rate is measured, and feedback is provided to the pump to ensure the required flow rate is achieved. A filter is fixed downstream of the flow meter to remove any impurities prior to the preheater. The fluid enters the preheater (Bulk Heater Module, BHM) which adds heat to raise the enthalpy of working fluid such that the desired inlet quality to the FBM is realized. The fluid enters the FBM either as a subcooled liquid or saturated two-phase mixture, gains heat and leaves as either a subcooled liquid or two-phase mixture. The fluid rejects all gained heat in a fluid-to-water heat exchanger to a condensing water loop and exits as a subcooled liquid. To ensure thermodynamic uniformity, the fluid passes through a static mixer before reentering the pump. An air-pressurized accumulator connected via a T-junction between the mixer and pump maintains a set reference pressure and helps suppress two-phase instabilities [64]. A degassing contactor, used to remove non-condensable gases, is provided in parallel immediately after the accumulator T-junction.

The static mixer, present before the pump, is incorporated in the flow loop exclusively in the present configuration. In the parabolic flight data, recorded during parabolic maneuvers on a Boeing 727 aircraft to provide brief periods of microgravity, deaeration was done prior to installing the facility on the aircraft. This was accomplished by utilizing the preheater to boil the working fluid, coupled with a partially filled fluid container plumbed into the system at the fill and drain ports where non-condensable gases are vented out. Upon exiting the pump, fluid passed through the filter prior to a turbine flow meter. A liquid-to-air heat exchanger was used to condense the fluid. The accumulator used in this system was nitrogen filled.

In both the 2014 and 2015 experiments, fluid entered the filter prior to the flow meter, which was of Coriolis and turbine types, respectively. For 2015 data, two smaller preheaters were used as opposed to a single preheater, and the accumulator was replaced by a reservoir at atmospheric pressure. For 2016 data, fluid entered the filter prior to a turbine flow meter, and the condenser was a liquid-to-air heat exchanger.

3. Assessment of Existing CHF Correlations

3.1. CHF database

Datasets from prior years were merged to form the consolidated FBCE-CHF database. It spans a wide range of operating conditions and is comprised of data for single- and double-sided heating in both microgravity with subcooled inlet, and Earth gravity with subcooled and saturated inlet conditions at a variety of orientations. A summary of the database is provided in Table 1, providing parametric ranges for each individual dataset, as well as the complete database. Table 2 shows relevant thermophysical properties of nPFH within the pressure range of the current database, obtained from NIST-REFPROP [65]. FC-72 is comprised of a specific combination of perfluorohexane isomers and its most prominent component is nPFH (73.2%) [63]. Fig. 4 shows the percentage difference in relevant thermophysical properties of FC-72 (provided by 3M company) from nPFH (obtained from NIST-REFPROP [65]). The maximum percent difference between the two fluids in the current operating range for pertinent properties is less than 6%. Therefore, the two fluids will perform similarly and will be referred to synonymously.

In the following subsections, a variety of flow boiling CHF correlations presently available in the literature will be used to predict q''_{CHF} for the current database. Correlations are segregated by whether they are intended for subcooled, saturated CHF, or both, and will be compared to the corresponding subset of the database. Even though the FBM, with a $Co = 0.195 - 0.216$ for the subcooled MST data [62] is clearly a macro-channel [66], correlations designed for flow boiling CHF in single (not parallel) micro-, mini-, or macro-channels are evaluated to assess if the flow physics contributing to CHF in the present channel conforms to that experienced in development of the tested correlations. This can provide valuable insight into meaningful, or meaningless, terms present in each correlation. Previously, many researchers developed correlations for flow through circular cross sections. In order to apply these correlations to the current database, the hydraulic diame-

Table 1
Summary of consolidated FBCE-CHF database.

Datasets	Testing Fluid	Heating Configuration	Flow Orientation/ Environment	N	G [kg/m^{2}s]	$\dot{m}$ [g/s]	p_{in} [kPa]	T_{in}[°C]	$\Delta T_{sub,in}$[°C]	$x_{e,in}$	p_{out} [kPa]	T_{out} [°C]	$\Delta T_{sub,out}$[°C]	$x_{e,out}$	q''_{CHF} [W/cm^2]
Parabolic flight (2013) data	FC-72	Single-sided	μg	10	226.02	2.83	117.19	58.74	2.75	-0.081	116.65	60.10	0.00	-0.022	13.26
					−3019.17	−37.74	−150.02	−63.35	−5.88	−0.036	−150.89	−63.56	−3.67	−0.099	−34.10
		Double-sided	μg	20	210.11	2.63	109.77	51.01	1.87	-0.125	108.07	56.87	0.00	-0.002	19.42
					−3050.29	−38.13	−166.84	−65.54	−9.55	−0.025	−151.55	−66.42	−3.88	−0.436	−37.62
2014 data	FC-72	Single-sided	Horizontal (bottom)	22	99.09	1.24	98.51	28.35	0.00 −28.31	-0.362	96.70	34.52	0.00	-0.308	23.80
					−3199.29	−39.99	−173.37	−73.99		−0.004	−159.11	−67.74	−23.07	−0.355	−42.31
			Horizontal (top)	21	211.37	2.64	97.12	28.55	0.00	-0.401	95.68	31.88	0.00	-0.302	6.30
					−3200.20	−40.00	−170.81	−73.42	−31.17	−0.003	−158.13	−67.48	−25.22	−0.081	−42.89
		Double-sided	Horizontal	23	144.24	1.80	97.10	28.44	0.79	-0.354	96.51	37.45	0.00	-0.292	6.82
					−3211.55	−40.14	−184.40	−74.91	−27.84	−0.011	−164.16	−69.17	−19.69	−0.093	−42.60
2015 data	FC-72	Single-sided	Horizontal (bottom)	32	192.52	2.41	115.28	54.44	0.00	0.00	113.92	59.89	0.00	0.028	11.31
					−2027.52	−25.34	−184.26	−76.87	−0.00	−0.633	−158.69	−66.83	−0.00	−0.779	−21.88
			Horizontal (top)	32	194.89	2.44	114.17	57.36	0.00	0.00	113.24	56.56	0.00	0.031	3.77
					−2029.99	−25.37	−180.72	−77.29	−0.00	−0.658	−157.57	−66.78	−0.00	−0.720	−23.09
			Vertical up	32	193.08	2.41	110.33	54.22	0.00	0.00	108.02	57.84	0.00	0.031	8.38
					−1977.40	−24.72	−181.75	−79.10	−0.00	−0.686	−153.74	−66.55	−0.00	−0.794	−23.09
			Vertical down	32	199.34	2.49	119.38	58.88	0.00	0.00	114.83	59.66	0.00	0.027	6.48
					−2030.27	−25.38	−182.29	−80.60	−0.00	−0.668	−154.38	−66.52	−0.00	−0.766	−23.09
		Double-sided	Horizontal	32	183.49	2.29	114.96	55.29	0.00	0.00	113.61	56.92	0.00	0.058	4.05
					−1999.62	−25.00	−191.75	−78.68	−0.00	−0.635	−162.54	−67.12	−0.00	−0.781	−21.44
			Vertical up	32	197.13	2.46	109.71	54.57	0.00	0.00	106.93	58.99	0.00	0.058	8.82
					−1963.43	−24.54	−190.27	−80.00	−0.00	−0.678	−157.90	−67.16	−0.00	−0.901	−22.48
			Vertical down	28	200.97	2.51	120.28	58.09	0.00	0.00	116.61	61.40	0.00	0.053	8.26
					−1991.39	−24.89	−191.20	−81.30	−0.00	−0.656	−159.02	−66.94	−0.00	−0.866	−21.44
2016 data	FC-72	Double-sided	Horizontal	19	183.71	2.30	106.23	23.15	0.00	-0.455	107.42	39.57	0.00	-0.391	7.74
					−2389.54	−29.87	−221.04	−78.75	−35.63	−0.195	−215.65	−78.27	−23.49	−0.394	−50.81
			Vertical up	19	175.30	2.19	122.27	26.12	0.00	-0.477	120.79	40.83	0.00	-0.495	19.13
					−2435.41	−30.44	−229.77	−79.43	−36.67	−0.157	−223.68	−79.62	−29.01	−0.567	−50.56
			Vertical down	19	201.85	2.52	107.20	27.93	0.00	-0.495	107.81	37.84	0.00	-0.420	6.15
					−2314.43	−28.93	−239.48	−79.60	−37.54	−0.183	−234.23	−79.00	−27.93	−0.482	−46.95
MST data	nPFH	Single-sided	Vertical up	23	179.70	2.25	119.89	34.32	0.00	-0.420	113.22	39.94	0.00	-0.269	14.18
					−3199.97	−40.00	−171.17	−76.90	−31.65	−0.518	−167.90	−71.41	−20.51	−0.607	−50.62
		Double-sided	Vertical up	21	179.75	2.25	125.44	35.80	0.00	-0.429	119.66	45.25	0.00	-0.198	14.19
					−3199.96	−40.00	−190.81	−79.37	−32.00	−0.404	−172.75	−72.12	−17.13	−0.613	−43.58
Overall	nPFH, FC-72	Single-sided and double-sided	$1g_e$ (vertical up, vertical down, horizontal) and μg	417	99.09	1.24	97.10	23.15	0.00	-0.495	95.68	31.88	0.00	-0.495	4.05
					−3211.55	−40.14	−239.48	−81.30	−37.54	−0.686	−234.23	−79.62	−29.01	−0.901	−50.81

Table 2
Thermophysical properties of nPFH.

p [kPa]	T_{sat} [°C]	ρ_f [kg/m^3]	ρ_g [kg/m^3]	h_f [J/kg]	h_g [J/kg]	h_{fg} [J/kg]	σ [mN/m]
90.00	53.67	1589.39	11.88	-3785.44	81668.53	85453.96	8.54
140.00	67.02	1546.18	18.17	10956.26	92547.97	81591.71	7.26
190.00	77.06	1511.96	24.49	22239.61	100754.35	78514.74	6.38
240.00	85.24	1482.73	30.87	31558.99	107434.00	75875.01	5.70

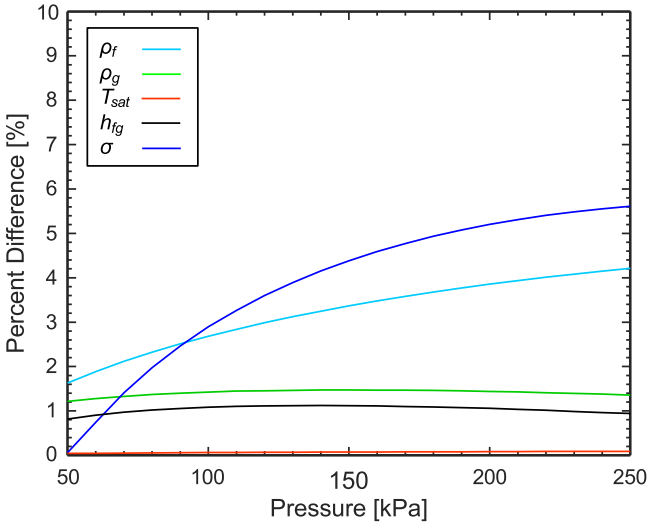

Fig. 4. Percentage difference in thermophysical properties of FC-72 from nPFH.

ter of the channel is used inplace of the diameter. For correlations that specifically call for another diameter or length scale defined by original authors, the corresponding value is used. The accuracy of each correlation is assessed by its mean absolute error, MAE, which is calculated for N datapoints as

$$MAE(\%) = \frac{1}{N}\sum\left|\frac{q''_{CHF,pred} - q''_{CHF,exp}}{q''_{CHF,exp}}\right| \times 100. \quad (1)$$

Some correlations are designed for specific flow orientations, however, predictions are made for all orientations in Earth gravity and microgravity. The only exception is microgravity data will be excluded for correlations that result in zero or singularity as g approaches zero, to not unnecessarily increase their MAEs. The overall MAE of each correlation will be used to determine the most accurate correlation for the database. To fairly assess each correlation, MAEs will also be presented for each orientation and heating configuration, as some correlations may perform significantly better for a specific condition, for example, vertical upflow with single-sided heating.

3.2. Assessment of subcooled CHF correlations

A variety of correlations for subcooled CHF are presented in Table 3 , along with remarks regarding the correlation development and intended use. Parity plots of the six best performing correlations are shown in Fig. 5. The two best performing correlations with MAEs of 21.47% and 27.06% are Shah's correlation for vertical [34] and horizontal flows [36], respectively. These correlations were developed for a wide range of operating conditions and 23 fluids with vastly different thermophysical properties, and proved capable at predicting the current database with reasonable accuracy. However, one shortcoming is the inability to predict microgravity data because the paramount parameter Y becomes singular when gravitational acceleration is set to zero. Interestingly, the correlation for vertical upflow outperforms the correlation for horizontal flow even for the horizontal data. In general, Shah's correlation for vertical upflow underpredicts the current database at all orientations. The inclusion of the multiplier for horizontal flow, which takes values between 0 and 1 to capture the lower q''_{CHF} experienced for horizontal flow as compared to vertical upflow, decreases the prediction of q''_{CHF} further and increases the error compared to the correlation designed for vertical upflow. The correlation by Shibahara *et al.* [67], originally developed for subcooled water, also produced good predictions with an overall MAE of 27.88% with slight overpredictions. It was developed by modifying the correlation of Hata *et al.* [68] to predict q''_{CHF} for lower outlet subcoolings and account for the influence of pressure. Even though the original correlation of Hata *et al.* [68] is designed for water with $\Delta T_{sub,out} \geq 30$°C, it still predicts the present database reasonably well with an overall MAE of 40.34%. The correlation of Celata *et al.* [26] predicts subcooled CHF with an overall MAE of 33.83%, performing significantly worse for vertical upflow with an MAE >20% more than horizontal flow or microgravity. Similar to the correlations by Shah, the CHF database was generally underpredicted. The lack of a term to accommodate the higher q''_{CHF} experienced for vertical upflow caused its MAE to suffer as underpredictions were more severe. One unique correlation that performed reasonably well is by Wright *et al.* [69], which produced an MAE of 42.50%. They accounted for conjugate heat transfer between the fluid and solid in their correlation while preserving the dependence of other fundamental parameters such as Weber number, Jacob number, and ratio between phase densities.

Outside of the six best performing correlations, a wide range of MAE is obtained for the others. Hall and Mudawar provided two pairs of correlations, one based on inlet quality and the other on outlet quality, for subcooled CHF of water flow boiling for ultra-high-flux applications [70] and their entire database [20]. These correlations share a common functional form, with the inlet-condition correlations derived from an energy balance in conjunction with the outlet correlation. This group of correlations all performed similarly, with the ultra-high-flux outlet correlation performing the best with an overall MAE of 46.65%. Tso *et al.* [71] took the form by Maddox and Mudawar [72] and proposed a correlation for a broader range of data that fit their vertical upflow data of FC-72 flowing over series of 10 mm×10 mm chips. The current database was predicted with an MAE of 61.02%, however, bottom-sided heating, vertical upflow, and microgravity data were predicted very well with MAEs of 12.10%, 10.48%, and 7.58%, respectively. The correlation was developed for FC-72 vertical upflow data but does not account for gravity itself and predicts significantly better for orientations that gravity does not adversely impact CHF, such as top-sided heating and vertical downflow. Kureta and Akimoto [56] developed a correlation for a rectangular channel exposed to single-sided heating and modified it to account for a variety of configurations including double-sided heating and circular tubes with fully circumferential and half-circumferential heating. To accomplish this, they proposed Bo to be dependent on We, Re, $x_{e,out}$, and P_h/P_w. However, this correlation was developed for water with a much narrower range of $x_{e,out}$ than the FBCE database and predicts it with an MAE of 96.84%. Hata *et al.* [73] modified their previous correlation [68] to utilize inlet subcooling instead of outlet subcooling and included an exponential term that varies with

Table 3
Correlations applicable to subcooled CHF.

Author(s)	Correlation	Remarks	Recommended/Validated Applicability Ranges
Becker *et al.* (1972) [78]	$q''_{CHF} = \frac{G(450+(h_f-h_{in}))}{40\frac{L_h}{D}+156G^{0.45}}(1.02-(p_r-0.54)^2)$ G is in kg/m^{2}s, h is in kJ/kg, $q"_{CHF}$ is in W/cm^2	• Based on inlet conditions • Water • Vertical upflow • Circular tubes • Developed using 515 datapoints	D = 10 mm L = 2000 –5000 mm G = 2000 –7000 kg/m^{2}s p = 120 –200 bar $\Delta T_{sub,in}$ = 8 –272°C $x_{e,out}$ = -0.3 – 0.6 $q"_{CHF}$ = 13 – 353 W/cm^2
Shah (1987) [34]	$Y = \left(\frac{GDc_{p,f}}{k_f}\right)\left(\frac{G^2}{\rho_f^2 gD}\right)^{0.4}\left(\frac{\mu_f}{\mu_g}\right)^{0.6}$ If $Y \le 10^6$ or $L_{CHF} > \frac{160}{p_r^{1.14}}$, or the fluid is helium, use the UCC. If $Y > 10^6$, use the correlation that gives the lower value of Bo. Upstream condition correlation (UCC): $Bo_{CHF} = 0.124\left(\frac{D}{L_E}\right)^{0.89}\left(\frac{10^4}{Y}\right)^n(1-x_{IE})$ $n = \begin{cases} 0, & Y \le 10^4 \\ (D/L_E)^{0.33}, & Y > 10^4 \text{and helium} \\ (D/L_E)^{0.54}, & 10^4 < Y \le 10^6 \text{and fluids other than helium} \\ \frac{0.12}{(1-x_{IE})^{0.5}}, & Y > 10^6 \text{and fluids other than helium} \end{cases}$ The effective length and inlet quality are defined as $L_E = \begin{cases} L_{CHF}, & x_{e,in} \le 0 \\ L_B, & x_{e,in} > 0 \end{cases}$ and $x_{IE} = \begin{cases} x_{e,in}, & x_{e,in} \le 0 \\ 0, & x_{e,in} > 0 \end{cases}$ For uniformly heated tubes, $\frac{L_B}{D} = \frac{x_{e,CHF}}{4Bo} = \frac{L_{CHF}}{D} + \frac{x_{e,in}}{4Bo}$ Local condition correlation (LCC): $Bo_{CHF} = F_E F_x Bo_o$ $F_E = \max\{1, \quad 1.54 - 0.032(\frac{L_{CHF}}{D})\}$ $Bo_o = \max\{15Y^{-0.612}, 0.082Y^{-0.3}(1+1.45p_r^{4.03}), 0.0024Y^{-0.105}(1+1.15p_r^{3.39})\}$ $c = \begin{cases} 0, & p_r \le 0.6 \\ 1, & p_r > 0.6 \end{cases}$; $F_x = F_1(1-\frac{(1-F_2)(p_r-0.6)}{0.35})^c$ $F_1 = \begin{cases} 1+0.0052(-x_{e,CHF}^{0.88})Y^{0.41}, & Y \le 1.4\times10^7 \\ 1+0.0052(-x_{e,CHF}^{0.88})(1.4\times10^7)^{0.41}, & Y > 1.4\times10^7 \end{cases}$; $F_2 = \begin{cases} F_1^{-0.42}, & F_1 \le 4 \\ 0.55, & F_1 > 4 \end{cases}$	• Consists of 2 correlations: upstream condition correlation (UCC) and local conditions correlation (LCC) • UCC based on inlet conditions • LCC based on conditions where CHF occurs which is usually the outlet • Water, R-11, R-12, R-21, R-22, R-113, R-114, ammonia, hydrazine, N_2O_4, MIPD, CO_2, helium, nitrogen, hydrogen, acetone, benzene, diphenyl, ethanol, ethylene glycol, o-terphenyl, potassium, rubidium • Vertical upflow • Uniformly heated tubes • Developed using a consolidated database of 1443 datapoints	D = 0.32 – 37.8 mm L_{CHF}/D = 1.3 – 940 G = 4 – 29051 kg/m^{2}s p_r = 0.0014 – 0.962 $x_{e,in}$ = -4.0 – 0.81 $x_{e,CHF}$ = -2.6 – 1.0 $q"_{CHF}$ = 0.11 – 45000 kW/m^2 Y = 6 – 720000000 For helium only: D = 0.47 – 4.05 mm L_{CHF}/D = 5.0 – 194.0 G = 10 – 630 kg/m^{2}s p_r = 0.43 – 0.89 $x_{e,in}$ = -0.53 – 0.8 $x_{e,out}$ = -0.23 – 1.0 $q"_{CHF}$ = 0.11 – 5.9 kW/m^2 Y = 10000 – 4400000
Nariai & Inasaka (1989) [79]	$Bo_{CHF} = \frac{C'}{\text{Re}^{0.5}}$; $C = 1.76 - 7.43x_{e,out} + 12.22x_{e,out}^2$ $C' = C[1 - \frac{52.3+80x_{e,out}-50x_{e,out}^2}{60+(p\times10^{-5})^{1.4}}]$ p is in Pa	• Based on outlet conditions • Water • Not orientation-specific • Uniformly heated circular tubes • Validated for a consolidated database of ~150 datapoints	D = 2 – 20 mm L_h = 50 – 2000 mm G = 1350 – 20000 kg/m^{2}s p = 0.1 – 20 MPa
Celata *et al.* (1994) [26]	$Bo_{CHF} = \frac{C}{\text{Re}^{0.5}}$; $C = (0.216 + 4.74\times10^{-2}p)\Psi$ p is in MPa $\Psi = \begin{cases} 1, & x_{e,out} < -0.1 \\ 0.825 + 0.986x_{e,out}, & -0.1 < x_{e,out} < 0 \\ 1/(2+30x_{e,out}), & x_{e,out} > 0 \end{cases}$	• Based on outlet conditions • Water • Not orientation-specific • Small diameter circular channels • Validated for a consolidated database of 1865 datapoints	D = 0.3 – 25.4 mm L_h = 2.5 – 610 mm G = 900 – 90000 kg/m^{2}s p = 0.1 – 8.4 MPa T_{in} = 0.3 – 242.7°C $q"_{CHF}$ = 3.3 – 227.9 MW/m^2
Vandervort *et al.* (1994) [28]	$q''_{CHF} = 17.05(G')^{0.0732+0.239D'}$ $\times(T')^{0.3060(G')+0.001730(T')-0.0353(D')}$ $\times(p')^{-0.1289}$ $\times(1+0.01213(D')^{-2.946+0.7821(G')+0.009299(T')})$ $\times(1.540-1.280(L/D)')$ $G' = 0.005 + \frac{G}{10^5}$; $T' = 5 + \Delta T_{sub,out}$; $p' = \frac{0.0333+p}{3.0}$; $D' = \frac{D}{0.003}$ $(L/D)' = \frac{(L_h/D)}{40}$ G is in kg/m^{2}s, T is in°C, p is in MPa, D is in m, $q"_{CHF}$ is in W/m^2	• Based on outlet conditions • Water • Not orientation-specific • Uniformly heated circular tubes • Developed using a consolidated database of 721 *high-heat-flux* datapoints ($q"_{CHF}$ ~10^7 – 2×10^8 W/m^2)	D = 0.3 – 3.0 mm L/D = 1.0 – 40.0 G = 3000 – 90000 kg/m^{2}s p = 0.1 – 3.0 MPa $\Delta T_{sub,out}$ = 0 – 200°C $q"_{CHF}$ = 6×10^6 – 2×10^8 W/m^2
Hall & Mudawar (1999) [70]	Based on outlet quality: $Bo_{CHF} = a_3 We_D^{c_1}\left(\frac{\rho_f}{\rho_g}\right)^{b_3}\left[1-\frac{a_4}{a_3}\left(\frac{\rho_f}{\rho_g}\right)^{b_4-b_3}x_{e,out}\right]$ Based on pseudo-inlet quality (recommended): $Bo_{CHF} = \frac{a_3 We_D^{c_1}\left(\frac{\rho_f}{\rho_g}\right)^{b_3}[1-\frac{a_4}{a_3}\left(\frac{\rho_f}{\rho_g}\right)^{b_4-b_3}x^*_{e,in}]}{1+4a_4 We_D^{c_1}\left(\frac{\rho_f}{\rho_g}\right)^{b_4}\left(\frac{L_h}{D}\right)}$ $x^*_{e,in} = \frac{h_{in}-h_{f,out}}{h_{fg,out}}$ $a_3 = 0.0332$; $a_4 = 0.0227$; $b_3 = -0.681$; $b_4 = 0.151$; $c_1 = -0.235$	• Developed 2 correlations: one based on outlet quality, and the other based on pseudo-inlet quality derived from energy balance between inlet and outlet • Based on outlet conditions • Water • Vertical upflow and horizontal flow • Uniformly heated circular tubes • Validated for a consolidated database of 1596 *high-heat-flux* datapoints • Correlation form determined from parametric trends observed in database	D = 0.25 – 15.0 mm L/D = 1.7 – 97 G = 1500 – 134000 kg/m^{2}s p_{out} = 0.7 – 196 bar $\Delta T_{sub,in}$ = 13 – 347°C $x_{e,in}$ = -2.47 – -0.04 $\Delta T_{sub,out}$ = 1 – 305°C $x_{e,out}$ = -2.13 – 0.00 $q"_{CHF}$ = 4 – 276 MW/m^2

(*continued on next page*)

Table 3 (*continued*)

Author(s)	Correlation	Remarks	Recommended/Validated Applicability Ranges
Hall & Mudawar (2000) [20]	Based on outlet quality: $Bo_{CHF} = C_1 We_D^{C_2}\left(\frac{\rho_f}{\rho_g}\right)^{C_3}\left[1 - C_4\left(\frac{\rho_f}{\rho_g}\right)^{C_5} x_{e,out}\right]$ Based on psuedo-inlet quality (recommended): $Bo_{CHF} = \frac{C_1 We_D^{C_2}\left(\frac{\rho_f}{\rho_g}\right)^{C_3}\left[1-C_4\left(\frac{\rho_f}{\rho_g}\right)^{C_5} x^*_{e,in}\right]}{1+4C_1C_4We_D^{C_2}\left(\frac{\rho_f}{\rho_g}\right)^{C_3+C_5}\left(\frac{L_h}{D}\right)}$ $x^*_{e,in} = \frac{h_{in}-h_{f,out}}{h_{fg,out}}$ $C_1 = 0.0722$; $C_2 = -0.312$; $C_3 = -0.644$; $C_4 = 0.900$; $C_5 = 0.724$	• Developed 2 correlations: one based on outlet quality, and another derived from energy balance between inlet and outlet based on pseudo-inlet quality • Based on outlet conditions • Water • Vertical upflow and horizontal flow • Uniformly heated circular tubes • Outlet correlation can be used for tubes heated with axial nonuniformity • Validated for a consolidated database of 4860 datapoints • Correlation form determined from parametric trends observed in database	D = 0.25 – 15.0 mm L/D = 2 – 200 G = 300 – 30000 kg/m^{2}s p_{out} = 1 – 200 bar $x_{e,in}$ = -2.0 – 0.0 $x_{e,out}$ = -1.0 – 0.05 (outlet quality correlation) $x_{e,out}$ = -1.0 – 0.00 (psuedo-inlet quality correlation)
Tso *et al.* (2000) [71]	$\frac{q''_{CHF}}{\rho_g U h_{fg}} = 0.203 We_L^{\frac{-11}{23}}\left(\frac{\rho_f}{\rho_g}\right)^{\frac{15}{23}}\left(\frac{L_h}{D_h}\right)^{\frac{1}{23}}\left(1+\frac{c_{p,f}\Delta T_{sub,in}}{h_{fg}}\right)^{\frac{7}{23}} \times\left(1+0.021\frac{\rho_f}{\rho_g}\frac{c_{p,f}\Delta T_{sub,in}}{h_{fg}}\right)^{\frac{16}{23}}$	• Based on inlet conditions • FC-72 • Vertical upflow • Rectangular channel • Developed using 16 datapoints	We_L = 1 – 1000
Kureta & Akimoto (2002) [56]	$Bo_{CHF} = \frac{C_1(x_{e,out}+C_2)}{Ca^{0.5}}$ $C_1 = \left(6.9\left(\frac{P_h}{P_w}\right)^2 - 10\left(\frac{P_h}{P_w}\right)+2\right)\times 10^{-3}$; $C_2 = -0.75\left(\frac{P_h}{P_w}\right)^2 + 0.9\left(\frac{P_h}{P_w}\right) - 0.28$ $x_{e,out} = x_{e,in} + \frac{P_h L_h}{A}\frac{q''_{CHF}}{G h_{fg}}$	• Based on outlet conditions • Water • Not orientation-specific • Rectangular channels subjected to single- and double-sided heating and tubes with half- and full-circumferential heating • Validated for a consolidated database of 407 datapoints	D = 1.0 – 7.8 mm L = 10 – 200 mm P_h/P_w = 0.25 – 1.0 G = 1000 – 2000 kg/m^{2}s T_{in} = 5 – 90°C $x_{e,out}$ = -0.163 – 0.0099 q''_{CHF} = 1.0 – 70.0 MW/m^2
Hata *et al.* (2004) [68]	$Bo_{CHF} = 0.082\left(\frac{D}{\sqrt{\frac{\sigma}{g(\rho_f-\rho_g)}}}\right)^{-0.1} We_D^{-0.3}\left(\frac{L_h}{D}\right)^{-0.1}\left(\frac{c_{p,f}\Delta T_{sub,out}}{h_{fg}}\right)^{0.7}$	• Based on outlet conditions • Water • Vertical upflow • Short circular tubes • Validated for a consolidated database of 1284 datapoints	D = 0.33 – 12 mm U = 4 – 60 m/s p_{out} = 0.159 – 3.1 MPa $\Delta T_{sub,out}$ = 30 – 205°C
Hata *et al.* (2006) [73]	$Bo_{CHF} = C_1\left(\frac{D}{\sqrt{\frac{\sigma}{g(\rho_f-\rho_g)}}}\right)^{-0.1} We_D^{-0.3}\left(\frac{L_h}{D}\right)^{-0.1}\exp\left(-\frac{(L_h/D)}{C_2 Re^{0.4}}\right)\left(\frac{c_{p,f}\Delta T_{sub,in}}{h_{fg}}\right)^{C_3}$ If $L_h/D \le 40$, $C_1 = 0.082$; $C_2 = 0.53$; $C_3 = 0.7$ If $L_h/D > 40$, $C_1 = 0.092$; $C_2 = 0.85$; $C_3 = 0.9$	• Based on outlet conditions • Water • Vertical upflow • Short circular tubes • Validated for a consolidated database of 1805 datapoints	D = 2 – 12 mm L_h = 22 – 150 mm U = 4.0 – 13.3 m/s p_{in} = 0.159 – 1.0 MPa $\Delta T_{sub,in}$ = 40 – 151°C $\Delta T_{sub,out}$ = 30 – 140°C
Sarma *et al.* (2006) [74]	$Bo_{CHF} = 0.118 Re^{-0.23} p_r^{0.2}\left(\frac{D}{L_h}\right)^{0.45}\left(\frac{c_{p,f}\Delta T_{sub}}{h_{fg}}\right)$	• Based on inlet conditions • Water and R-12 • Not orientation-specific • Small diameter circular tubes • Validated for a consolidated database consisting of 2718 datapoints	D = 0.25 – 37.5 mm L_h =1.77 – 2300 mm G = 385.3 – 90000 kg/m^{2}s p = 0.953 – 206.69 bar T_{in} = 1.5 – 354.03°C q''_{CHF} = 1.104 – 227.95 MW/m^2
Wright *et al.* (2008) [69]	$q''_{CHF} = q^* h_{fg}\sqrt{\lambda\rho_g g(\rho_f-\rho_g)} q^* \frac{P_h L_h}{A} = 3.9\left(\frac{k_f\rho_f c_{p,f}}{k_s\rho_s c_{p,s}}\right)^{0.5}\left(1+\left(\frac{\rho_g}{\rho_f}\right)^{0.1}\right)^{-6.7} We_D^{-0.33} Bi\left(1+\frac{(h_f-h_{in})}{h_{fg}}\right)G^* + 0.018$ $G^* = \frac{G}{\sqrt{\lambda\rho_g g(\rho_f-\rho_g)}}$; $\lambda = \sqrt{\frac{\sigma}{g(\rho_f-\rho_g)}}$ $Bi = \frac{hL_c}{k_s}$; $L_c = \sqrt{\frac{V_s}{H}}$; $h = 6.4\times 10^6 (Bo^{2.1} We_D)^{0.28}\left(\frac{\rho_g}{\rho_f}\right)^{0.21}$	• Based on inlet conditions • Water • Aluminum channel • Vertical upflow • Single and multiple rectangular channels based on the Advanced Test Reactor at Idaho National Laboratory • Developed using a consolidated database of 126 datapoints • Considers effects produced by combinations of fluid and solid	G = 9.5 – 110 kg/m^{2}s p = 10.3 – 344 kPa T_{in} = 18 – 71°C
Roday & Jensen (2009) [77]	$Bo_{CHF} = \frac{C_1 We_D^{C_2}\left(\frac{\rho_f}{\rho_g}\right)^{C_3}\left(\frac{L_h}{D}\right)^{C_4}(x_{e,in}+C_5)}{(We_D+C_6)\left(\frac{L_h}{D}+C_7\right)}$ $C_1 = 44587$; $C_2 = 1.136$; $C_3 = -0.625$; $C_4 = -1.680$; $C_5 = -0.0157$; $C_6 = -0.425$; $C_7 = -279.8$	• Based on inlet conditions • Water • Not orientation-specific • Circular micro-tubes • Developed using 41 datapoints	L_h/D = 75 – 200 We_D = 0.46 – 20.01 ρ_f/ρ_g = 930 – 6022 $x_{e,in}$ = -0.149 – -0.053

(*continued on next page*)

Table 3 (*continued*)

Author(s)	Correlation	Remarks	Recommended/Validated Applicability Ranges
Shah (2015) [36]	$q''_{CHF} = K_{hor} q''_{CHF,vert}$ $K_{hor} = \begin{cases} 1, & x_{e,in} < 0 \text{and } L_{CHF}/D < 10 \\ \min(0.725 Fr_f^{0.082}, 1), & x_{e,CHF} \le 0.05 \\ \min(0.64 Fr_{TP}^{0.15}, 1), & x_{e,CHF} > 0.05 \end{cases}$ $Fr_f = \frac{G^2}{\rho_f^2 gD}$; $Fr_{TP} = \frac{x_{e,CHF} G}{\sqrt{\rho_g(\rho_f - \rho_g) gD}}$	• Conditions used depend on $q''_{CHF,vert}$ correlation • Water, FC-72, HFE-7100, R-12, R-31, R-113, R-134a, R-123, R-236fa, R-245fa • Horizontal flow • Single and parallel channels with circular or rectangular geometries subject to uniform or nonuniform heating • Validated for a consolidated database of 878 datapoints • Converts q''_{CHF} predictions for vertical upflow to horizontal flow • Recommends Shah (1987) for $q''_{CHF,vert}$ but can be applied to other vertical tube CHF correlations	D = 0.13 – 24.3 mm L_{CHF}/D = 1.97 – 488 G = 20 – 11390 kg/m^{2}s p_r = 0.0053 – 0.900 $x_{e,in}$ = -1.05 – 0.72 $x_{e,CHF}$ = -0.2 – 0.99
Shibahara *et al.* (2017) [67]	$Bo_{CHF} = 0.149\left(\frac{\rho_f}{\rho_g}\right)^{-0.47} D^{*-0.1} We_D^{-0.3} \left(\frac{L_h}{D}\right)^{-0.1} \left(\frac{\rho_f c_{p,f} \Delta T_{sub,out}}{\rho_g h_{fg}}\right)^{0.14}$ $D^* = \frac{D}{\sqrt{\frac{\sigma}{g(\rho_f - \rho_g)}}}$	• Based on outlet conditions • Water • Circular tubes • Vertical upflow • Validated for a consolidated database of > 450 datapoints	D = 0.92 – 6.0 mm L_h/D = 2.5 – 40.9 U = 4.3 – 30.6 m/s
Ping *et al.* (2021) [76]	If $L_h/D_h \le 100$, $q''_{CHF} = (163.87 + \exp(4.4509 - 0.0538 D_h))$ $\times(0.1356 + \exp(-1.29 - 0.0111 \frac{L_h}{D_h}))$ $\times(-1.5335 + \exp(0.7498 - 0.0082 p))$ $\times(-1.2428 + \exp(0.1288 - 1.852 \times 10^{-5} G))$ $\times(-6.6239 + \exp(1.8 + 0.64 x_{e,in}))$ $-(0.2263 - 6.1166 x_{e,in} - 1.7282 x_{e,in}^2)$ If L_h/D_h >100, $q''_{CHF} = (-1.40066 + \exp(0.3281 + 0.00017 D_h))$ $\times(44.19 + \exp(4.906 - 0.0081 \frac{L_h}{D_h}))$ $\times(-10.965 + \exp(2.316 + 0.00093 p))$ $\times(-7.4785 + \exp(1.83 - 2 \times 10^{-4} G))$ $\times(-2.937 + \exp(0.574 + 1.883 x_{e,in}))$ $-(1.56 - 0.77 x_{e,in} - 0.32 x_{e,in}^2)$ D_h is in mm, L_h is in mm, G is in Mg/m^{2}s, p is in MPa, q''_{CHF} is in MW/m^2	• Based on inlet conditions • Water • Vertical upflow and horizontal flow • Uniformly and nonuniformly heated circular tubes • Developed from a consolidated database of 1318 datapoints	D = 1– 36 mm L_h/D = 12 – 365 G = 700 – 40000 kg/m^{2}s p = 0.3 – 19 MPa $x_{e,in}$ = -2.4 – -0.18 q''_{CHF} = 2 – 60 MW/m^2
Ganesan *et al.* (2021) [75]	$Bo_{CHF} = \begin{cases} 0.0425 We_D^{-0.21} (\frac{\rho_f}{\rho_g})^{-0.32} (1 - x_{e,in})^{2.07} (\frac{L_{CHF}}{D})^{-0.41}, & \alpha_{CHF} < 0.6 \\ 0.225 We_D^{-0.22} (\frac{\rho_f}{\rho_g})^{-0.19} (1 - x_{e,in})^{2.68} (\frac{L_{CHF}}{D})^{-0.79}, & \alpha_{CHF} \ge 0.6 \end{cases}$ $\alpha_{CHF} = (1 + (\frac{1 - x_{e,CHF}}{x_{e,CHF}})(\frac{\rho_g}{\rho_f})^{\frac{2}{3}})^{-1}$	• Based on inlet conditions • Hydrogen, helium, nitrogen, methane • Not orientation-specific • Uniformly heated circular tubes • Developed from a consolidated database of 2312 datapoints	D = 0.5 – 14.1 mm L_{CHF}/D = 2.5 – 230.8 G = 2.2 – 8203.9 kg/m^{2}s p_{in} = 0.01 – 4.07 MPa p_r = 0.1 – 0.93 $\Delta T_{sub,in}$ = 0 – 78.9°C $x_{e,in}$ = -2.06 – 0.95 $x_{e,CHF}$ = -1.23 – 1.00 q''_{CHF} = 0.05 – 8203.9 kW/m^2

both L_h/D and Re. This term varies in the range of 0.012 – 0.348 for the current database, however, it was formulated with data featuring higher velocities and higher Re than the current database resulting in values of 0.243 – 0.941, which would lessen its impact. Inclusion of this term coupled with underpredciton of the original correlation worsened the results to an MAE of 81.05%. The correlation by Sarma *et al.* [74], which captures subcooling by calculating properties based on inlet temperature, produces an MAE of 46.88%. Their correlation was developed for water and R-12, and assumed CHF was caused by evaporation of the liquid layer between a slug bubble and the liquid wall. However, in previous studies [42,46,57,58,60], the observed mechanism was lift-off of wetting fronts in the troughs of a wavy vapor layer forming along the heated wall. The CHF correlation for cryogenic fluids developed by Ganesan *et al.* [75] predicted the current database with an MAE of 63.86%. Some properties of cryogenic fluids are vastly different than nPFH, and can have over an order of magnitude difference, resulting in inaccurate predictions. Irrespective of this, the functional form of the correlation contains common parameters and trends.

Some correlations completely lack the ability to even remotely predict q''_{CHF} for the current database with MAEs of 100% or greater. Two of these are empirical correlations that were developed by statistical fits to high-heat-flux data on the order of 10^6 – 10^7 W/m^2, while the present data is of the order 10^4 – 10^5 W/m^2. The correlation by Ping *et al.* [76] produced the highest overall MAE of 1973.14%. The predicted q''_{CHF} values are an order of magnitude higher than the database, reflecting the range of data the correlation was tuned to. To the opposite effect, the correlation by Vandervort *et al.* [28], that was developed for heat fluxes and flow rates that exceed those of the current database, vastly underpredicts q''_{CHF}, resulting in an MAE of 100% at all orientations. It is obvious the combination of the form and the data used to develop these correlations hinders their accuracy for the current database. The correlation by Roday and Jensen [77] also produced an abnormally large MAE of 517.94%. Clearly this correlation does not effectively capture trends of the current database. One noticeable feature of the correlation is Bo scales with $We^{0.136}$. This differs from the correlations by Shibahara *et al.* [67], Hata *et al.* [68], and Wright *et al.* [69] that scaled Bo, to good effect, with We raised to a power in the range of -0.33 – -0.3. The dimensional correlation by Becker *et al.* [78], developed for high pressure water, p > 120 bar, resulted in an MAE of 202.24%. Not only are the relatively low-pressure data in this database well below the minimum recommended for the correlation, but the reduced

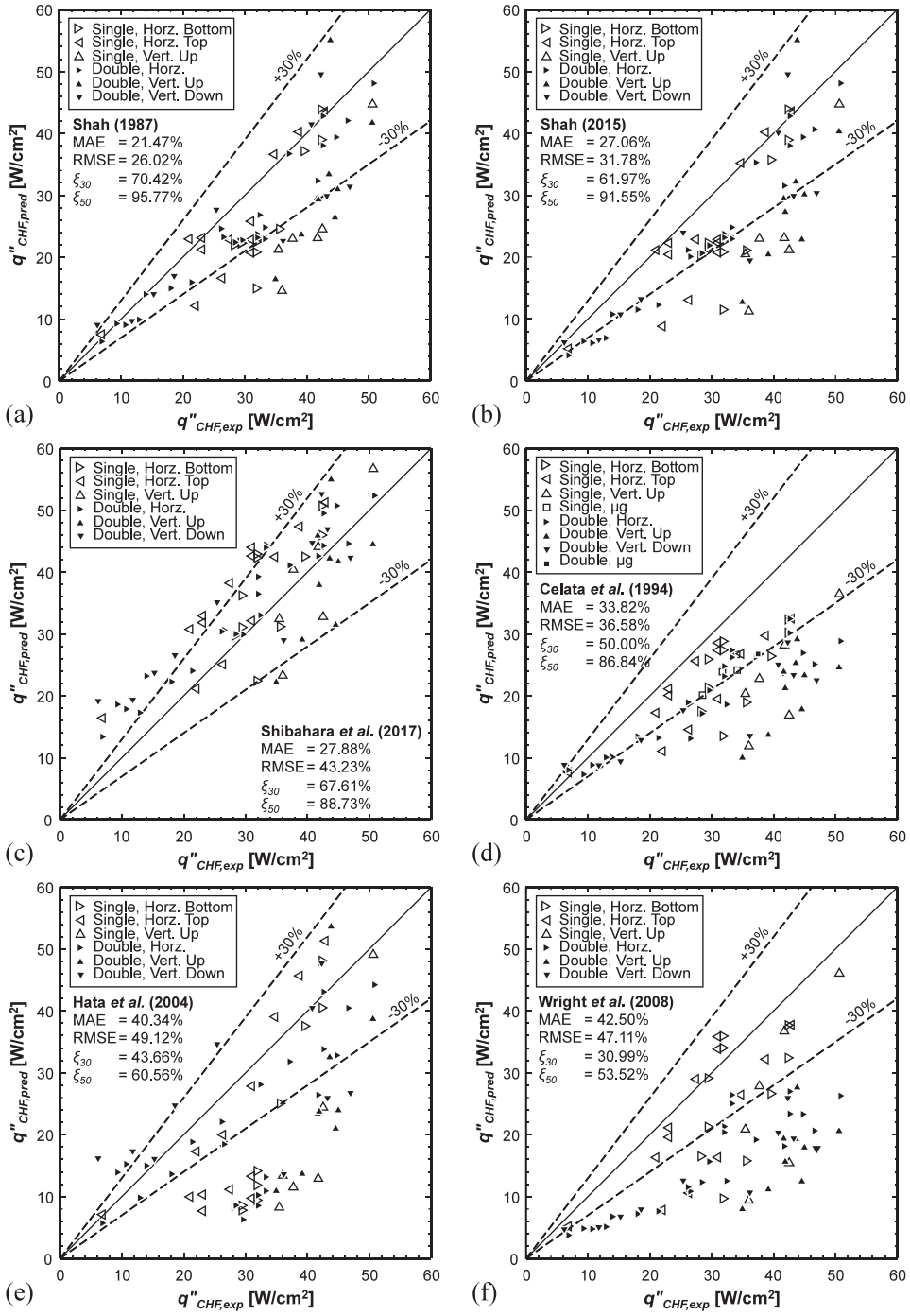

Fig. 5. Parity plots of the six best performing correlations for subcooled CHF: (a) Shah (1987) [34], (b) Shah (2015) [36], (c) Shibahara *et al.* (2017) [67], (d) Celata *et al.* (1994) [26], (e) Hata *et al.* (2004) [68], and (f) Wright *et al.* (2008) [69].

pressures, which are featured in the correlation, are also significantly lower. The correlation is recommended for p =120 – 200 bar which corresponds to p_r = 0.54 – 0.91 for water, while the current database contains a max p_r = 0.138. Similar to Celata *et al.* [26], Nariai and Inasaka [79] modified the coefficient of the Tong correlation as a function of pressure and outlet quality to better fit their lower-pressure water data. However, it is less accurate in predicting the current database with an MAE of 135.46%. Their database was ~10% of the size of the database of Celata *et al.*, with lesser variations in mass velocity and subcooling, possibly hindering the correlation when extrapolating it to other conditions. More details regarding the overall MAE of each correlation, as well as the MAE for each configuration are included in Table 4.

3.3. Assessment of saturated CHF correlations for single-phase inlet

Table 5 provides details of correlations designed for saturated CHF, including remarks regarding their development and intended use. The MAEs of saturated CHF has been divided into single-phase and two-phase inlet conditions, and are presented respectively in Table 6 and Table 7.

Table 4
MAEs of subcooled-CHF correlations.

	Horizontal Flow				Vertical Upflow			Vertical Downflow			μg Flow			Overall
Author(s)	Bottom	Top	Double	Overall	Single	Double	Overall	Single	Double	Overall	Single	Double	Overall	
Becker *et al.* (1972) [78]	232.96	260.29	202.31	225.36	176.94	128.99	148.17	-	176.95	176.95	304.66	327.10	309.15	202.24
Shah (1987) [34]	23.59	16.33	14.70	17.09	39.55	32.24	35.16	-	21.06	21.06	-	-	-	21.47
Nariai & Inasaka (1989) [79]	106.61	106.62	139.94	121.58	76.07	145.79	117.90	-	225.67	225.67	54.25	61.33	55.67	135.46
Celata *et al.* (1994) [26]	28.95	21.42	30.48	27.58	45.02	51.47	48.89	-	39.95	39.95	26.18	28.58	26.66	33.83
Vandervort *et al.* (1994) [28]	100.00	100.00	100.00	100.00	100.00	100.00	100.00	-	100.00	100.00	100.00	100.00	100.00	100.00
Hall & Mudawar (1999) [70] (Inlet)	67.16	67.26	60.96	64.09	71.83	57.94	63.50	-	49.66	49.66	81.37	75.74	80.24	61.93
Hall & Mudawar (1999) [70] (Outlet)	53.27	52.76	35.95	44.47	62.06	54.75	57.67	-	40.18	40.18	78.78	82.00	79.42	46.65
Hall & Mudawar (2000) [20] (Inlet)	62.99	62.90	56.12	59.53	68.31	52.85	59.03	-	43.41	43.41	77.96	72.04	76.78	57.16
Hall & Mudawar (2000) [20] (Outlet)	51.99	46.15	45.59	47.14	54.71	49.55	51.61	-	65.03	65.03	70.45	75.24	71.41	50.60
Tso *et al.* (2000) [71]	12.10	55.21	88.17	62.32	12.18	9.35	10.48	-	130.85	130.85	6.31	12.66	7.58	61.02
Kureta & Akimoto (2002) [56]	124.03	126.34	78.53	101.93	118.87	81.53	96.47	-	73.98	73.98	117.90	92.40	112.80	96.84
Hata *et al.* (2004) [68]	45.52	36.07	33.88	37.03	53.95	43.54	47.70	-	44.50	44.50	-	-	-	40.34
Hata *et al.* (2006) [73]	80.88	82.22	81.26	81.45	83.14	78.93	80.61	-	79.86	79.86	-	-	-	81.05
Sarma *et al.* (2006) [74]	46.63	45.21	45.83	45.83	54.25	51.99	52.89	-	43.06	43.06	48.37	37.04	46.10	46.88
Wright *et al.* (2008) [69]	28.20	24.94	48.55	37.45	37.67	61.01	51.67	-	51.97	51.97	-	-	-	42.50
Roday & Jensen (2009) [77]	444.30	397.88	509.80	463.93	472.38	693.49	605.04	-	635.76	635.76	317.99	710.76	396.54	517.94
Shah (2015) [36]	26.94	20.05	24.59	23.82	42.78	36.59	39.07	-	23.96	23.96	-	-	-	27.06
Shibahara *et al.* (2017) [67]	18.04	35.52	26.09	27.01	15.23	17.68	16.70	-	48.65	48.65	-	-	-	27.88
Ping *et al.* (2021) [76]	1250.43	1789.22	2462.45	2008.71	1104.11	1408.92	1287.00	-	3365.13	3365.13	925.99	897.82	920.36	1973.14
Ganesan *et al.* (2021) [75]	66.27	62.95	62.66	63.53	70.73	68.21	69.22	-	57.32	57.32	65.76	61.82	64.97	63.86

Table 5
Correlations applicable to saturated CHF.

Author(s)	Correlation	Remarks	Recommended/Validated Applicability Ranges
Becker *et al.* (1972) [78]	$q''_{CHF} = \frac{G(450+(h_f-h_{in}))}{40\frac{L_h}{D}+156G^{0.45}}(1.02-(p_r-0.54)^2)$ G is in kg/m^{2}s, h is in kJ/kg, q''_{CHF} is in W/cm^2	• Based on inlet conditions • Water • Vertical upflow • Circular tubes • Developed using 515 datapoints	D = 10 mm L = 2000 – 5000 mm G = 2000 – 7000 kg/m^{2}s p = 120 – 200 bar $\Delta T_{sub,in}$ = 8 – 272°C $x_{e,out}$ = -0.3 – 0.6 q''_{CHF} = 13 – 353 W/cm^2 δ > 0.07
Green (1982) [89]	$q''_{CHF} = 0.25\rho_g u_g h_{fg}\frac{D}{L_s}\frac{1}{1+\delta}$ $\delta = 0.046(\frac{L_h}{D})^{1.12}(\frac{D}{L_s})^{1.65}e^{25000LFN-0.038\frac{\rho_f}{\rho_g}}$ $LFN = \frac{G\sigma}{\rho_f\mu_f h_{fg}}$ L_s is saturated boiling length	• Assumed constant pressure • Water and Freon 12 • Vertical upflow • Uniformly heated circular tubes • Developed using a consolidated database of 233 datapoints	
Katto & Ohno (1984) [30]	$q''_{CHF} = q''_o(1+K\frac{(h_f-h_{in})}{h_{fg}})$ If ρ_g/ρ_f < 0.15: $q''_o = \begin{cases} q''_{o2}, & q''_{o2} < q''_{o3} \\ \max(q''_{o3}, q''_{o4}), & q''_{o2} > q''_{o3} \end{cases}$; $K = \max(\ K_6,\ K_7\ )$ If ρ_g/ρ_f > 0.15: $q''_o = \begin{cases} q''_{o2}, & q''_{o2} < q''_{o13} \\ \max(q''_{o13}, q''_{o5}), & q''_{o2} > q''_{o13} \end{cases}$; $K = \begin{cases} K_6, & K_6 > K_7 \\ \min(K_7, K_9), & K_6 < K_7 \end{cases}$ $\frac{q''_{o2}}{Gh_{fg}} = CWe_L^{-0.043}\frac{D}{L_h}$; $\frac{q''_{o3}}{Gh_{fg}} = 0.10(\frac{\rho_g}{\rho_f})^{0.133}We_L^{-\frac{1}{3}}\frac{1}{1+0.0031\frac{L_h}{D}}$ $\frac{q''_{o4}}{Gh_{fg}} = 0.098(\frac{\rho_g}{\rho_f})^{0.133}We_L^{-0.433}\frac{(\frac{L_h}{D})^{0.27}}{1+0.0031\frac{L_h}{D}}$ $\frac{q''_{o5}}{Gh_{fg}} = 0.0384(\frac{\rho_g}{\rho_f})^{0.6}We_L^{-0.173}\frac{1}{1+0.28We_L^{-0.233}\frac{L_h}{D}}\frac{q''_{o13}}{Gh_{fg}} =$ $0.234(\frac{\rho_g}{\rho_f})^{0.513}We_L^{-0.433}\frac{(\frac{L_h}{D})^{0.27}}{1+0.0031\frac{L_h}{D}}$ $C = \begin{cases} 0.25, & L_h/D < 50 \\ 0.25+0.0009(\frac{L_h}{D}-50), & 50 \le L_h/D \le 150 \\ 0.34, & L_h/D > 150 \end{cases}$ $K_6 = (\frac{1.043}{4CWe_L^{-0.043}})$; $K_7 = (\frac{5(0.0124+\frac{D}{L_h})}{6(\frac{\rho_g}{\rho_f})^{0.133}We_L^{-\frac{1}{3}}})$ $K_8 = 0.416(\frac{(0.0221+\frac{D}{L_h})(\frac{D}{L_h})^{0.27}}{(\frac{\rho_g}{\rho_f})^{0.133}We_L^{-0.433}})$; $K_9 = 1.12(\frac{1.52We_L^{-0.233}+\frac{D}{L_h}}{(\frac{\rho_g}{\rho_f})^{0.6}We_L^{-0.173}})$	• Based on inlet conditions • Water, anhydrous ammonia, benzene, ethanol, helium I, para-hydrogen, monoisopropylbiphenyl, nitrogen, potassium, R-12, R-21, R-22, R-113, R-114, R-115 • Vertical upflow • Uniformly heated circular tubes • Validated for a consolidated database consisting of > 1000 datapoints	D = 1 – 38.1 mm L_h/D = 5 – 940 ρ_g/ρ_f = 0.00027 – 0.517
Shah (1987) [34]	$Y = (\frac{GDc_{p,f}}{k_f})(\frac{G^2}{\rho_f^2 gD})^{0.4}(\frac{\mu_f}{\mu_g})^{0.6}$ If $Y \le 10^6$ or $L_{CHF} > \frac{160}{p_r^{1.14}}$, or the fluid is helium, use the UCC. If $Y > 10^6$, use the correlation that gives the lower value of Bo. Upstream condition correlation (UCC): $Bo_{CHF} = 0.124(\frac{D}{L_E})^{0.89}(\frac{10^4}{Y})^n(1-x_{IE})$ $n = \begin{cases} 0, & Y \le 10^4 \\ (D/L_E)^{0.33}, & Y > 10^4 \text{and helium} \\ (D/L_E)^{0.54}, & 10^4 < Y \le 10^6 \text{and fluids other than helium} \\ \frac{0.12}{(1-x_{IE})^{0.5}}, & Y > 10^6 \text{and fluids other than helium} \end{cases}$ The effective length and inlet quality are defined as $L_E = \begin{cases} L_{CHF}, & x_{e,in} \le 0 \\ L_B, & x_{e,in} > 0 \end{cases}$ and $x_{IE} = \begin{cases} x_{e,in}, & x_{e,in} \le 0 \\ 0, & x_{e,in} > 0 \end{cases}$ For uniformly heated tubes, $\frac{L_B}{D} = \frac{x_{e,CHF}}{4Bo} = \frac{L_{CHF}}{D} + \frac{x_{e,in}}{4Bo}$ Local condition correlation (LCC): $Bo_{CHF} = F_E F_x Bo_o$ $F_E = \max\{1,\ 1.54-0.032(\frac{L_{CHF}}{D})\}$ $Bo_o = \max\begin{Bmatrix} 15Y^{-0.612}, 0.082Y^{-0.3}(1+1.45p_r^{4.03}), \\ 0.0024Y^{-0.105}(1+1.15p_r^{3.39}) \end{Bmatrix}$ $c = \begin{cases} 0, & p_r \le 0.6 \\ 1, & p_r > 0.6 \end{cases}$ $F_x = F_3(1+\frac{(F_3^{-0.29}-1)(p_r-0.6)}{0.35})^c$; $F_3 = (\frac{1.25\times10^5}{Y})^{0.833x_{e,CHF}}$	• Consists of 2 correlations: upstream condition correlation (UCC) and local conditions correlation (LCC) • Conditions used depend on case • Water, R-11, R-12, R-21, R-22, R-113, R-114, ammonia, hydrazine, N_2O_4, MIPD, CO_2, helium, nitrogen, hydrogen, acetone, benzene, diphenyl, ethanol, ethylene glycol, o-terphenyl, potassium, rubidium • Vertical upflow • Uniformly heated tubes • Developed using a consolidated database of 1443 datapoints	D = 0.32 – 37.8 mm L_{CHF}/D = 1.3 – 940 G = 4 – 29051 kg/m^{2}s p_r = 0.0014 – 0.962 $x_{e,in}$ = -4.0 – 0.81 $x_{e,CHF}$ = -2.6 – 1.0 q''_{CHF} = 0.11 – 45000 kW/m^2 Y = 6 – 720000000 For helium only: D = 0.47 – 4.05 mm L_{CHF}/D = 5.0 – 194.0 G = 10 – 630 kg/m^{2}s p_r = 0.43 – 0.89 $x_{e,in}$ = -0.53 – 0.8 $x_{e,out}$ = -0.23 – 1.0 q''_{CHF} = 0.11 – 5.9 kW/m^2 Y = 10000 – 4400000
Oh & Englert (1993) [88]	$q''_{CHF} = q^* h_{fg}\sqrt{\lambda\rho_g g(\rho_f-\rho_g)}$ Vertical upflow: $(\frac{A_h}{A})q^* = 0.458(1+\frac{(h_f-h_{in})}{h_{fg}})G^* + 2.412$ Vertical downflow: $(\frac{A_h}{A})q^* = 0.406(1+\frac{(h_f-h_{in})}{h_{fg}})G^* + 2.412$ $G^* = \frac{G}{\sqrt{\lambda\rho_g g(\rho_f-\rho_g)}}$; $\lambda = \sqrt{\frac{\sigma}{g(\rho_f-\rho_g)}}$	• Based on inlet conditions (uses inlet subcooling) • Water • Vertical upflow and downflow • Thin rectangular channels with single-sided heating • Developed using 116 datapoints • Low flow rates used to simulate natural circulation	L_h = 609.6 mm L_h/D = 154 G = 30 – 80 kg/m^{2}s $\Delta T_{sub,in}$ = 5 – 72°C

(*continued on next page*)

Table 5 (*continued*)

Author(s)	Correlation	Remarks	Recommended/Validated Applicability Ranges
Celata *et al.* (1994) [26]	$Bo_{CHF} = \frac{C}{\mathrm{Re}^{0.5}}$; $C = (0.216 + 4.74 \times 10^{-2} p)\Psi$ $\Psi = \begin{cases} 1, & x_{e,out} < -0.1 \\ 0.825 + 0.986 x_{e,out}, & -0.1 < x_{e,out} < 0 \\ 1/(2 + 30 x_{e,out}), & x_{e,out} > 0 \end{cases}$ p is in MPa	• Based on outlet conditions • Water • Not orientation-specific • Small diameter circular channels • Validated for a consolidated database of 1865 datapoints	D = 0.3 – 25.4 mm L_h = 2.5 – 610 mm G = 900 – 90000 kg/m^{2}s P = 0.1 – 8.4 MPa T_{in} = 0.3 – 242.7°C $q"_{CHF}$ = 3.3 – 227.9 MW/m^2
Kureta & Akimoto (2002) [56]	$Bo_{CHF} = \frac{C_1 (x_{e,out} + C_2)}{Ca^{0.5}}$ $C_1 = \left(6.9\left(\frac{P_h}{P_w}\right)^2 - 10\left(\frac{P_h}{P_w}\right) + 2\right) \times 10^{-3}$; $C_2 = -0.75\left(\frac{P_h}{P_w}\right)^2 + 0.9\left(\frac{P_h}{P_w}\right) - 0.28$ $x_{e,out} = x_{e,in} + \frac{P_h L_h}{A} \frac{q"_{CHF}}{G h_{fg}}$	• Based on outlet conditions • Water • Not orientation-specific • Rectangular channels subjected to single- and double-sided heating and tubes with half- and full-circumferential heating • Validated for a consolidated database of 407 datapoints	D = 1.0 – 7.8 mm L = 10 – 200 mm P_h/P_w = 0.25 – 1.0 G = 1000 – 2000 kg/m^{2}s T_{in} = 5 – 90°C $x_{e,out}$ = -0.163 – 0.0099 $q"_{CHF}$ = 1.0 – 70.0 MW/m^2
Zhang *et al.* (2006) [29]	$Bo_{CHF} = 0.0352(We_D + 0.0119(\frac{L_h}{D_h})^{2.31}(\frac{\rho_g}{\rho_f})^{0.361})^{-0.295} \times (\frac{L_h}{D_h})^{-0.311}(2.05(\frac{\rho_g}{\rho_f})^{0.170} - x_{e,in})$	• Based on inlet conditions • Water • Not orientation-specific • Uniformly heated small diameter circular tubes • Developed from a consolidated database containing 3837 datapoints, of which 2539 are saturated • Database consists of both subcooled and saturated data • Hall & Mudawar (2000) was recommended for subcooled CHF predictions	D = 0.33 – 6.22 mm L/D = 1.0 – 975 p_{out} = .101 – 19.0 MPa G = 5.33 – 134000 kg/m^{2}s $x_{e,in}$ = -2.35 – 0.00 $x_{e,out}$ = -1.75 – 0.999 $q"_{CHF}$ = 0.00935 – 276 MW/m^2
Wojtan *et al.* (2006) [38]	$Bo_{CHF} = 0.437(\frac{\rho_g}{\rho_f})^{0.073} We_L^{-0.24}(\frac{L_h}{D})^{-0.72}$	• Based on inlet conditions • R-134a and R-245fa • Not orientation-specific • Single circular uniformly heated micro-channels • Developed using 34 datapoints	D = 0.50 – 0.80 mm L_h = 20 – 70 mm L_h/D = 25 – 141 G = 400 – 1600 kg/m^{2}s $\Delta T_{sub,in}$ = 2 – 15°C We_L = 293 – 21044 ρ_g/ρ_f = 0.009 – 0.041
Martin-Callizo *et al.* (2008) [85]	$Bo_{CHF} = 0.3216(\frac{\rho_g}{\rho_f})^{0.084} We_L^{-0.034}(\frac{L_h}{D})^{-0.942}$	• Based on inlet conditions • R-134a, R-22, R-245fa • Vertical upflow • Circular micro-channel • Developed using 12 datapoints	D = 0.640 mm L = 213 mm G = 180 – 535 kg/m^{2}s $x_{e,out}$ = 0.78 – 0.98 $q"_{CHF}$ = 24.95 – 68.71 kW/m^2
Koşar *et al.* (2009) [87]	$q"_{CHF} = a_0 D^{a_1 + a_2 D + a_3 \frac{L_h}{D} + a_4 G + a_5 p_{out} + a_6 (T_{sat,out} + \Delta T_{sub,out})} \times \frac{L_h}{D}^{a_7 + a_8 D + a_9 \frac{L_h}{D} + a_{10} G + a_{11} p_{out} + a_{12} (T_{sat,out} + \Delta T_{sub,out})} \times G^{a_{13} + a_{14} D + a_{15} \frac{L_h}{D} + a_{16} G + a_{17} p_{out} + a_{18} (T_{sat,out} + \Delta T_{sub,out})} \times p_{out}^{a_{19} + a_{20} D + a_{21} \frac{L_h}{D} + a_{22} G + a_{23} p_{out} + a_{24} (T_{sat,out} + \Delta T_{sub,out})} \times (T_{sat,out} + \Delta T_{sub,out})^{a_{25} + a_{26} D + a_{27} \frac{L_h}{D} + a_{28} G + a_{29} p_{out} + a_{30} (T_{sat,out} + \Delta T_{sub,out})}$ $a_0 = 1597831$, $a_1 = -1.599$, $a_2 = -2.114$, $a_3 = 2.611 \times 10^{-3}$, $a_4 = -7.361 \times 10^{-8}$, $a_5 = 3.265 \times 10^{-4}$, $a_6 = -4.017 \times 10^{-3}$, $a_7 = -0.419$, $a_8 = -5.025 \times 10^{-3}$, $a_9 = -6.553 \times 10^{-4}$, $a_{10} = 3.292 \times 10^{-6}$, $a_{11} = -3.047 \times 10^{-4}$, $a_{12} = 1.863 \times 10^{-3}$, $a_{13} = 0.478$, $a_{14} = -1.266 \times 10^{-2}$, $a_{15} = 1.909 \times 10^{-4}$, $a_{16} = -7.493 \times 10^{-6}$, $a_{17} = -1.407 \times 10^{-4}$, $a_{18} = -1.269 \times 10^{-3}$, $a_{19} = 1.571$, $a_{20} = -0.138$, $a_{21} = 1.761 \times 10^{-3}$, $a_{22} = 1.529 \times 10^{-5}$, $a_{23} = 6.802 \times 10^{-4}$, $a_{24} = -1.187 \times 10^{-2}$, $a_{25} = -4.888$, $a_{26} = 0.975$, $a_{27} = -7.617 \times 10^{-4}$, $a_{28} = -6.728 \times 10^{-7}$, $a_{29} = -3.583 \times 10^{-4}$, $a_{30} = 1.686 \times 10^{-2}$ $q"_{CHF}$ is in W/cm^2, L_h is in mm, D is in mm, G is in kg/m^{2}s, p_{out} is in kPa, $T_{sat,out}$ is in °C, ΔT_{out} is in °C	• Based on outlet conditions • Water • Circular channels • Not orientation-specific • Developed using a consolidated database of 364 datapoints	D = 0.127 – 2.7 mm L = 20 – 80 mm G = 1200 – 53000 kg/m^{2}s $x_{e,out}$ = -0.2 – 0.15
Tanaka *et al.* (2009) [81]	$q"_{CHF} = q^* h_{fg} \sqrt{\lambda \rho_g g (\rho_f - \rho_g)}$ $q^* = \frac{0.71^2 A \sqrt{\frac{W}{\lambda}}}{A_h (1 + (\frac{\rho_g}{\rho_f})^{0.25})^2} + 0.0047 G^* (\frac{L_h}{D_h})^{-0.31}$ $G^* \frac{G}{\sqrt{\lambda \rho_g g (\rho_f - \rho_g)}}$; $\lambda = \sqrt{\frac{\sigma}{g(\rho_f - \rho_g)}}$	• Based on inlet conditions • Water, R-134a, R-245fa • Not orientation-specific • Thin rectangular channels with double-sided heating and single circular uniformly heated mini-channels • Size of database is not specified. Data sources also do not specify number of datapoints	H = 1 – 2.8 mm L/D = 34 – 179 G = 0 – 200 kg/m^{2}s $\Delta T_{sub,in}$ = 20 – 80°C $x_{e,out}$ = 0.05 – 1.0

(*continued on next page*)

Table 5 (*continued*)

Author(s)	Correlation	Remarks	Recommended/Validated Applicability Ranges
Wu *et al.* (2011) [82]	$Bo_{CHF} = 0.60\left(\frac{L_h}{D_e}\right)^{-1.19} x_{e,out}^{0.817}$	• Based on outlet conditions • Water, R-236fa, R-134a, R-123, R-245fa, nitrogen • Not orientation-specific • Multi- and single- mini/micro-channels with circular and rectangular channels • Developed using a consolidated database of 595 datapoints	$L_h/D_e \leq 250$ $G \leq 4000$ kg/m^{2}s $p_{r,out} \leq 0.25$ $x_{e,out} = 0.05 - 1.00$ $BdRe_f^{0.5} \leq 200$
Wu & Li (2011) [83]	$Bo_{CHF} = \begin{cases} 0.62\left(\frac{L_h}{D_e}\right)^{-1.19} x_{e,out}^{0.82}, & \frac{L_h}{D_e} \leq 150 \\ 1.16\times10^{-3}\left(We_m Ca^{0.8}\right)^{-0.16}, & \frac{L_h}{D_e} > 150 \end{cases}$ $We_m = \frac{G^2 D_e}{\rho_m \sigma}$; $\rho_m = \frac{x_{e,out}}{\rho_g} + \frac{1-x_{e,out}}{\rho_f}$	• Based on outlet conditions • Water, R-236fa, R-134a, R-123, R-245fa, R-12, CO_2, nitrogen • Not orientation-specific • Multi- and single-, mini/micro-channels with circular and rectangular channels • Developed using a consolidated database of 859 datapoints	$BdRe_f^{0.5} = 0 - 200$
Basu *et al.* (2011)[84]	$Bo_{CHF} = 0.3784\left(\frac{\rho_g}{\rho_f}\right)^{0.051}\left(\frac{L_h}{D}\right)^{-1.03} x_{e,out}^{0.8}$	• Based on outlet conditions • R-134a, R-123 • Single circular micro-tubes • Not orientation-specific • Developed using a consolidated database of 193 datapoints	$D = 0.286 - 1.6$ mm $G = 300 - 1500$ kg/m^{2}s $\Delta T_{sub,in} = 5 - 40$°C $x_{e,out} = 0.3 - 1.0$
Ong & Thome (2011) [37]	$Bo_{CHF} = 0.12\left(\frac{\mu_f}{\mu_g}\right)^{0.183}\left(\frac{\rho_g}{\rho_f}\right)^{0.062} We_L^{-0.141}\left(\frac{L_h}{D_e}\right)^{-0.7}\left(\frac{D_e}{D_{th}}\right)^{0.11}$ $D_{th} = 2\sqrt{\frac{\sigma}{g(\rho_f-\rho_g)}}$	• Unspecified conditions • R-134a, R-236fa, R245fa • Not orientation-specific • Single-circular channels, rectangular multi-channels and split flow rectangular multi-channels • Developed using a consolidated database of 548 datapoints	$D = 0.35 - 3.04$ mm $L_h/D = 22.7 - 178$ $G = 84 - 3736$ kg/m^{2}s $We_L = 7 - 201232$ $\mu_f/\mu_g = 14.4 - 53.1$ $\rho_f/\rho_g = 0.024 - 0.036$
Tibiriçá *et al.* (2012) [80]	$q''_{CHF} = \min(q''_1, q''_2) \times (1 + \max(K_1, K_2)\frac{(h_f - h_{in})}{h_{fg}})$ $q''_1 = CGh_{fg}\left(\frac{\sigma\rho_f}{G^2 L_{eq}}\right)^{0.0298}\frac{D_{eq}}{L_{eq}}$ $q''_2 = 0.06213 Gh_{fg}\left(\frac{\rho_g}{\rho_f}\right)^{0.085}\left(\frac{\sigma\rho_f}{G^2 L_{eq}}\right)^{0.31348}\frac{1}{1+0.0031\frac{L_{eq}}{D_{eq}}}$ $K_1 = \frac{1.043}{4C\left(\frac{\sigma\rho_f}{G^2 L_{eq}}\right)^{0.043}}$; $K_2 = \frac{5(0.0124+\frac{D_{eq}}{L_{eq}})}{6\left(\frac{\rho_g}{\rho_f}\right)^{0.133}\left(\frac{\sigma\rho_f}{G^2 L_{eq}}\right)^{\frac{1}{3}}}$ $C = \begin{cases} 0.25, & L_{eq}/D_{eq} < 50 \\ 0.25 + 0.00076(L_{eq}/D_{eq} - 50), & 50 \leq L_{eq}/D_{eq} \leq 150 \\ 0.32576, & L_{eq}/D_{eq} > 150 \end{cases}$ $D_{eq} = \sqrt{\frac{4A}{\pi}}$; $L_{eq} = \frac{P_h L_h}{\pi D_{eq}}$	• Based on inlet conditions • R-134a, R-245fa, R-1234ze(E) • Horizontal flow • Uniformly heated elliptical tubes of different aspect ratios • Developed using a consolidated database of 150 datapoints	$D = 1.0 - 2.2$ mm $L_h = 90 - 361$ mm $\beta = 0.25 - 4$ $G = 100 - 1500$ kg/m^{2}s $\Delta T_{sub,in} = 4 - 10$°C
Mikielewicz (2013) [86]	$Bo_{CHF} = 0.62\left(\frac{\rho_g}{\rho_f}\right)^{-0.02} We_D^{-0.05}\left(\frac{L_h}{D}\right)^{-1.17}$	• Based on conditions averaged between inlet and outlet • R-123, R-134a, SES36, ethanol • Vertical upflow • Small diameter circular tubes	$D = 1.15 - 2.3$ mm $L_h = 375 - 385$ mm $G = 40 - 900$ kg/m^{2}s $p_{avg} = 0.4 - 6.8$ bar $x_{e,CHF} = 0.65 - 1.00$ $q''_{CHF} = 20 - 220$ kW/m^2
Shah (2015) [36]	$q''_{CHF} = K_{hor} q''_{CHF,vert}$ $K_{hor} = \begin{cases} 1, & x_{e,in} < 0 \text{ and } L_{CHF}/D < 10 \\ \min(0.725 Fr_f^{0.082}, 1), & x_{e,CHF} \leq 0.05 \\ \min(0.64 Fr_{TP}^{0.15}, 1), & x_{e,CHF} > 0.05 \end{cases}$ $Fr_f = \frac{G^2}{\rho_f^2 gD}$; $Fr_{TP} = \frac{x_{e,CHF} G}{\sqrt{\rho_g(\rho_f-\rho_g)gD}}$	• Conditions used depend on $q''_{CHF,vert}$ correlation • Water, FC-72, HFE-7100, R-12, R-31, R-113, R-134a, R-123, R-236fa, R-245fa • Horizontal flow • Single tubes and multi-channels with round and rectangular channels, uniform and nonuniform heating • Validated for a consolidated database of 878 datapoints • Converts q''_{CHF} predictions for vertical upflow to horizontal flow • Recommends Shah (1987) for $q''_{CHF,vert}$ but can be applied to other vertical tube CHF correlations	$D = 0.13 - 24.3$ mm $L_{CHF}/D = 1.97 - 488$ $G = 20 - 11390$ kg/m^{2}s $p_r = 0.0053 - 0.900$ $x_{e,in} = -1.05 - 0.72$ $x_{e,CHF} = -0.2 - 0.99$

(*continued on next page*)

Table 5 (*continued*)

Author(s)	Correlation	Remarks	Recommended/Validated Applicability Ranges
Tibiriçá *et al.* (2017) [18]	$Bo_{CHF} = 0.242We_{eq}^{-0.1635}\left(\frac{L_{eq}}{D_{eq}}\right)^{-0.6834}\left(\frac{\rho_g}{\rho_f}\right)^{0.0598}(1-x_{e,in})^{0.881}La^{-0.0714}$ $We_{eq} = \frac{G^2 D_{eq}}{\sigma \rho_f}$; $La = \frac{\sigma \rho_f D_{eq}}{\mu_f^2}$ $D_{eq} = \sqrt{\frac{4A}{\pi}}$; $L_{eq} = \frac{P_h L_h}{\pi D_{eq}}$	• Unspecified conditions • Water, R-12, R-123, R-134a, R-236fa, R-245fa, R-1234ze(E), nitrogen • Not orientation-specific • Circular and rectangular micro-channels • Developed using a consolidated database of 1110 datapoints	L_h/D = 20 – 500 $x_{e,in}$ = -0.6 – 0.15 We = .01 – 200000 ρ_f/ρ_g = 6.5 – 129000 La = 50000 – 6000000
Ganesan *et al.* (2021) [75]	$Bo_{CHF} = \begin{cases} 0.0425We_D^{-0.21}\left(\frac{\rho_f}{\rho_g}\right)^{-0.32}(1-x_{e,in})^{2.07}\left(\frac{L_{CHF}}{D}\right)^{-0.41}, & \alpha_{CHF} < 0.6 \\ 0.225We_D^{-0.22}\left(\frac{\rho_f}{\rho_g}\right)^{-0.19}(1-x_{e,in})^{2.68}\left(\frac{L_{CHF}}{D}\right)^{-0.79}, & \alpha_{CHF} \geq 0.6 \end{cases}$ $\alpha_{CHF} = \left(1+\left(\frac{1-x_{e,CHF}}{x_{e,CHF}}\right)\left(\frac{\rho_g}{\rho_f}\right)^{\frac{2}{3}}\right)^{-1}$	• Based on inlet conditions • Hydrogen, helium, nitrogen, methane • Not orientation-specific • Uniformly heated tubes • Developed using a consolidated database of 2312 datapoints	D = 0.5 – 14.1 mm L_{CHF}/D = 2.5 – 230.8 G = 2.2 – 8203.9 kg/m^{2}s p_{in} = 0.01 – 4.07 MPa p_r = 0.1 – 0.93 $\Delta T_{sub,in}$ = 0 – 78.9°C $x_{e,in}$ = -2.06 – 0.95 $x_{e,CHF}$ = -1.23 – 1.00 q''_{CHF} = 0.05 – 8203.9 kW/m^2

Parity plots of the six best performing correlations for saturated CHF with single-phase inlet are shown in Fig. 6. The best performing correlation is the one by Katto and Ohno [30] with an overall MAE of 32.36%. Vertical upflow produced the highest MAE of 37.37% and vertical downflow performed exceptionally well with an MAE of 15.34%, regardless of the correlation having been developed specifically for vertical upflow. The correlation by Zhang *et al.* [29], developed using a database of saturated CHF for water, predicted the saturated CHF data with an overall MAE of 35.63%. They developed their correlation form by taking inspiration from the form originally proposed by Katto [31], to better fit their water database with a single equation. Shah's generalized correlation for vertical upflow [34] again proves capable with a reasonable MAE of 39.29%, but, similar to the subcooled CHF data, generally underpredicted q''_{CHF}, again resulting in Shah's correlation for horizontal channels [36] to be slightly less accurate with an MAE of 49.52%. Another correlation that borrowed the functional form of Katto and Ohno is that by Tibiriçá *et al.* [80] which had an overall MAE of 39.99%. Tanaka *et al.* [81] proposed a correlation that assumes q''_{CHF} to be a combination of the flooding heat flux and a convective term. The dominance of the flooding phenomenon present in the correlation is not well extrapolated to the present database that contain mass velocities out of the recommended range of $G \leq$ 200 kg/m^{2}s. Regardless, their correlation still provides reasonable predictions with an MAE of 49.97%.

Others did not perform as well as the previously mentioned correlations in predicting saturated CHF for the current database. The correlation by Celata *et al.* [26], which provided relatively accurate predictions for subcooled CHF, predicted saturated CHF with an MAE of 79.64%. The correlation was not well tuned for saturated CHF as it was developed from data for subcooled CHF, but still applicable for saturated CHF. The simple dryout correlation of Wu *et al.* [82] produced an MAE of 83.00%, correlating Bo to $x_{e,out}$ and L_h/D ratio. Wu and Li [83] slightly modified the constants of [82] for $L_h/D \leq 150$ and developed a new correlation for L_h/D >150, which resulted in a slightly higher MAE of 86.24%. Basu *et al.* [84] developed their correlation, MAE = 72.83%, by fitting experimental data of R-123 and R-134a. Ganesan *et al.* [75] performed similarly for saturated CHF as it did for subcooled due to it being developed for cryogenic fluids.

The correlation by Ong and Thome [37], developed for microchannel heat sinks but specifically for refrigerants, produced an MAE of 592.52%. To create the correlation, they modified the correlation by Wojtan *et al.* [38], MAE = 106.82%, which is derived from the robust Katto and Ohno correlation but tweaked for their experimental data of refrigerants. The correlations by Martin-Callizo *et al.* [85] and Mikielwicz *et al.* [86], also altered Katto and Ohno's correlation for refrigerants, resulted in MAEs of 114.16% and 284.53, respectively. Overall, the scope of fluids used to develop these correlations is detrimental to their accuracy for the current database, especially when compared to their parent correlation that possesses a much broader range of applicability. Koşar *et al.* [87] took an approach similar to Vandervort *et al.* [28] and developed an empirical correlation featuring 31 constants. The data used to develop this correlation features orders of magnitude larger q''_{CHF} than the current database and predicts the current data with an overall MAE of 418.08%. Oh and Englert [88] proposed a correlation each for both vertical upflow and vertical downflow, both correlations failing to accurately predict the current database with respective MAEs of 378.08% and 328.98%. They found q''_{CHF} for vertical downflow to be 85% of vertical upflow for their experimental data, with this ratio being reflected from the coefficients although their two correlations have identical form. The experimental water data used to develop this correlation simulated natural convection that occurs in reactors during accidents. Therefore, the flow rates and pressures used in their experiments are below the scope of the present database, resulting in large overpredictions of q''_{CHF}. Green [89] developed a correlation, MAE = 259.39%, for low flow rates of G < 300 kg/m^{2}s and was validated for pressurized water and R-12. They used two unique dimensionless parameters, the Low Flow Number and defect factor to build their correlation, but it was not dependable in predicting the current database of nPFH. Tibiriçá *et al.* [18] developed a correlation for water, nitrogen, and refrigerants in horizontal micro-channels, which had an MAE of 121.67%. Correlations by Kureta and Akimoto [56] and Becker *et al.* [78] suffered similar issues as they did for subcooled CHF and produced respective MAEs of 107.78% and 247.58%.

3.4. Assessment of saturated CHF correlations for two-phase inlet

The saturated CHF data with two-phase inlet was compared to the same saturated CHF correlations, provided in Table 5. It can be seen in Table 7, which shows the MAEs of saturated CHF with two-phase inlet for different orientations, that no microgravity data is available with two-phase inlet. Similar to the previous two subsections, parity plots of the six correlations that provided the lowest overall MAEs are shown in Fig. 7. The correlation by Katto and Ohno [30] asserts itself as the best correlation for saturated CHF,

Table 6
MAEs of saturated-CHF correlations for single-phase inlet.

Author(s)	Horizontal Flow				Vertical Upflow			Vertical Downflow			μg Flow			Overall
	Bottom	Top	Double	Total	Single	Double	Total	Single	Double	Total	Single	Double	Total	
Becker *et al.* (1972) [78]	137.59	309.08	232.17	218.03	111.12	118.94	116.25	478.51	247.46	285.97	171.03	172.59	172.22	180.54
Green (1982) [89]	165.84	851.83	155.18	323.82	426.20	89.12	204.99	211.83	127.36	141.44	366.66	135.50	190.89	259.39
Katto & Ohno (1984) [30]	38.24	28.65	26.06	30.84	36.55	37.38	37.37	2.92	17.82	15.34	20.78	30.46	28.14	32.36
Shah (1987) [34]	45.96	48.75	27.61	30.58	49.22	53.59	52.09	8.68	29.65	26.15	-	-	-	39.29
Oh & Englert (1993) [88] Up	450.85	838.47	273.94	468.40	371.63	177.30	244.11	1505.13	323.73	520.63	-	-	-	378.08
Oh & Englert (1993) [88] Down	393.42	743.13	236.35	410.11	324.58	148.69	209.15	1329.53	279.17	454.23	-	-	-	328.98
Celata *et al.* (1994) [26]	82.64	55.49	75.52	73.21	85.23	88.98	87.69	53.96	82.14	77.44	74.20	83.08	80.95	79.64
Kureta & Akimoto (2002) [56]	105.03	117.71	102.29	106.88	104.09	110.54	108.32	119.76	108.69	110.53	110.16	104.50	105.86	107.78
Zhang *et al.* (2006) [29]	45.72	13.02	26.22	29.77	44.81	45.06	44.97	7.62	25.99	22.93	31.22	36.72	35.40	35.63
Wojtan *et al.* (2006) [38]	73.11	209.22	153.77	139.31	65.65	55.58	59.04	245.50	138.00	155.92	97.28	81.92	85.60	106.82
Martin-Callizo *et al.* (2008) [85]	104.57	173.51	115.74	125.60	70.53	93.77	85.78	386.06	154.50	193.09	88.75	117.92	110.92	114.16
Koşar *et al.* (2009) [87]	195.53	474.10	404.67	349.57	222.53	212.64	216.04	478.95	343.54	366.01	256.83	213.61	223.98	294.65
Tanaka *et al.* (2009) [81]	58.59	116.33	42.46	42.95	59.44	59.62	59.56	34.51	45.09	43.32	-	-	-	49.97
Wu *et al.* (2011) [82]	85.55	110.49	71.74	85.64	98.76	60.10	73.39	207.11	99.58	117.50	43.58	39.28	40.31	83.00
Wu & Li (2011) [83]	89.57	113.91	73.67	88.64	102.57	62.82	76.48	213.92	104.92	123.09	45.52	42.00	42.84	86.24
Basu *et al.* (2011) [84]	81.82	82.57	68.66	76.46	81.91	67.16	72.23	65.66	50.49	53.02	87.62	68.46	73.06	72.83
Ong & Thome (2011) [37]	643.46	1267.43	520.25	739.37	561.78	296.65	387.79	1791.50	546.94	754.37	-	-	-	592.52
Tibiriçá *et al.* (2012) [80]	32.78	116.33	42.42	56.63	23.84	19.25	20.83	88.80	26.49	36.88	47.55	18.81	25.71	39.99
Mikielewicz (2013) [86]	230.17	460.33	339.23	330.60	174.00	202.99	193.02	848.54	407.29	480.84	284.55	318.87	310.63	284.53
Shah (2015) [36]	55.02	16.02	41.51	40.09	60.79	63.47	62.55	8.68	45.95	39.74	-	-	-	49.52
Tibiriçá *et al.* (2017) [18]	127.84	309.25	104.00	160.77	105.23	49.09	68.38	430.86	103.71	158.24	175.30	74.55	98.73	121.67
Ganesan *et al.* (2021) [75]	71.31	64.23	53.07	61.95	66.56	58.64	61.36	56.61	56.52	56.53	65.53	56.97	59.02	61.28

Table 7
MAEs of saturated-CHF correlations for two-phase inlet.

Author(s)	Horizontal Flow				Vertical Upflow			Vertical Downflow			μg Flow			Overall
	Bottom	Top	Double	Overall	Single	Double	Overall	Single	Double	Overall	Single	Double	Overall	
Becker *et al.* (1972) [78]	178.66	360.57	288.75	276.52	229.17	194.35	210.89	280.60	219.62	249.62	-	-	-	247.58
Green (1982) [89]	110.64	206.17	155.66	157.42	132.63	104.01	117.60	160.90	115.28	137.73	-	-	-	138.98
Katto & Ohno (1984) [30]	21.96	51.90	32.57	35.36	12.86	16.83	14.94	22.65	13.95	18.23	-	-	-	24.06
Shah (1987) [34]	19.61	67.19	33.87	29.39	29.40	23.52	26.32	42.99	22.81	32.74	-	-	-	33.52
Oh & Englert (1993) [88] Up	522.00	887.02	310.68	562.41	630.28	217.74	413.70	728.26	242.57	481.56	-	-	-	491.62
Oh & Englert (1993) [88] Down	458.57	789.73	270.31	496.48	555.91	185.72	361.56	645.45	208.40	423.46	-	-	-	432.34
Celata *et al.* (1994) [26]	89.99	79.80	87.68	85.90	87.95	92.11	90.13	84.53	90.63	87.63	-	-	-	87.76
Kureta & Akimoto (2002) [56]	86.60	84.65	141.24	105.69	83.74	134.91	110.60	85.25	135.47	111.27	-	-	-	108.79
Zhang *et al.* (2006) [29]	44.57	32.21	30.05	35.38	35.73	40.65	38.31	24.66	33.88	29.34	-	-	-	34.77
Wojtan *et al.* (2006) [38]	108.96	272.09	210.44	197.71	147.80	122.49	134.51	197.32	147.44	171.99	-	-	-	169.89
Martin-Callizo *et al.* (2008) [85]	98.52	188.48	140.63	142.47	117.55	90.92	103.57	144.09	102.49	122.96	-	-	-	124.38
Koşar *et al.* (2009) [87]	289.05	617.13	512.23	474.43	362.27	329.63	345.13	468.07	381.18	423.94	-	-	-	418.08
Tanaka *et al.* (2009) [81]	42.66	15.95	31.96	30.27	31.88	46.67	40.17	21.46	43.63	32.72	-	-	-	34.21
Wu *et al.* (2011) [82]	545.03	819.87	330.86	555.59	688.01	275.17	471.27	701.76	280.02	487.54	-	-	-	509.62
Wu & Li (2011) [83]	564.01	846.72	343.74	574.88	711.38	286.51	488.32	725.23	291.46	504.90	-	-	-	527.66
Basu *et al.* (2011)[84]	42.44	36.05	31.82	36.57	42.41	32.69	37.31	36.20	35.21	35.70	-	-	-	36.59
Ong & Thome (2011) [37]	821.93	1445.42	632.62	952.88	989.20	447.31	704.71	1166.00	489.21	826.81	-	-	-	837.06
Tibiriçá *et al.* (2012) [80]	38.93	101.36	44.73	60.98	53.64	29.51	40.97	69.01	30.29	49.34	-	-	-	51.25
Mikielewicz (2013) [86]	279.20	498.85	397.49	392.08	345.59	286.86	314.76	403.37	316.11	359.05	-	-	-	357.63
Shah (2015) [36]	26.77	38.93	23.26	29.39	23.85	28.49	26.29	27.16	22.39	24.74	-	-	-	27.14
Tibiriçá *et al.* (2017) [18]	125.70	272.09	95.33	164.08	159.96	49.68	102.06	210.07	62.17	134.95	-	-	-	135.76
Ganesan *et al.* (2021) [75]	68.69	48.23	52.95	56.47	64.78	64.66	64.72	56.55	60.41	58.51	-	-	-	59.76

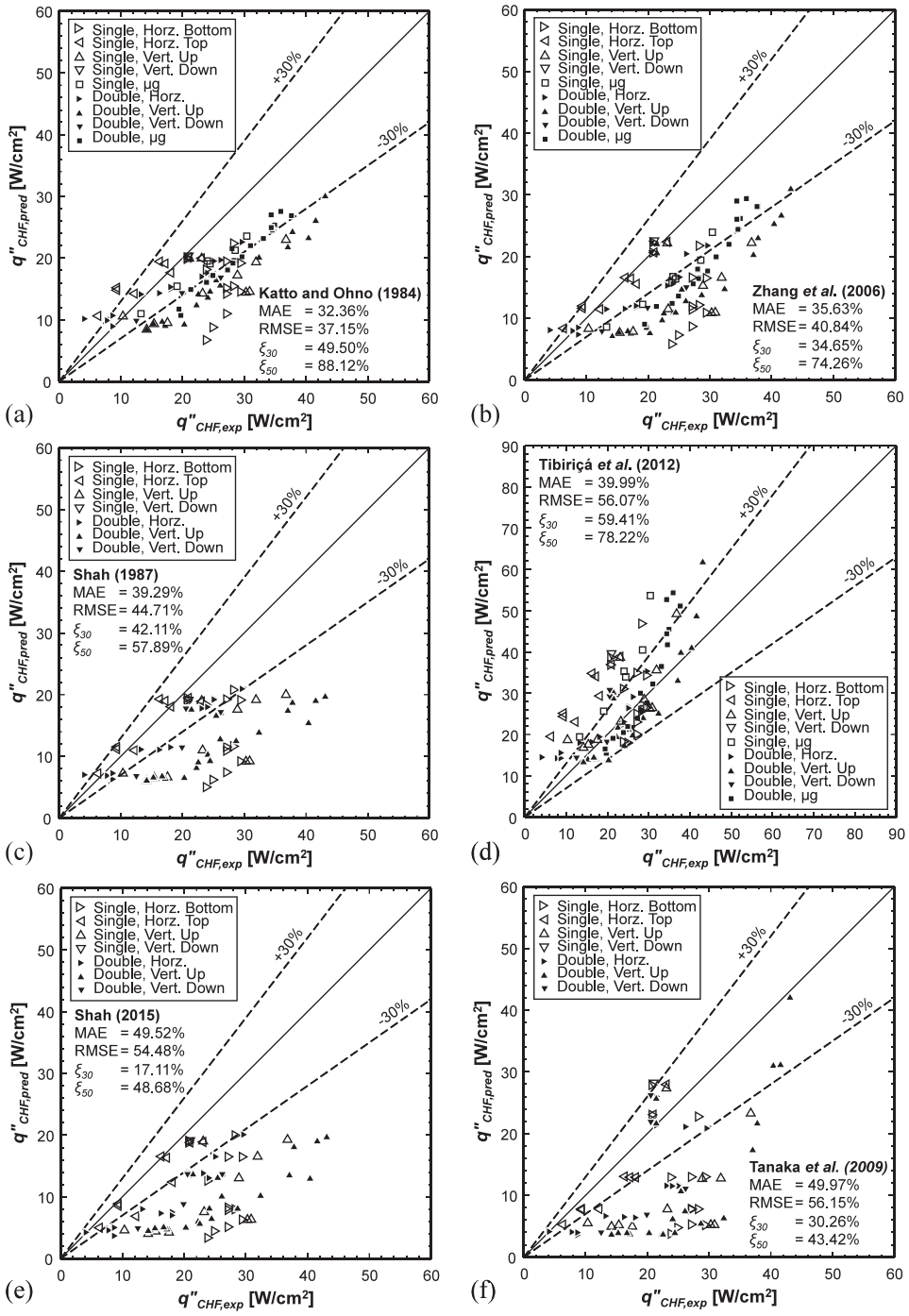

Fig. 6. Parity plots of the six best performing correlations for saturated CHF with single-phase (liquid) inlet: (a) Katto and Ohno (1984) [30], (b) Zhang *et al.* (2006) [29], (c) Shah (1987) [34], (d) Tibiriçá *et al.* (2012) [80], (e) Shah (2015) [36], and (f) Tanaka *et al.* (2009) [81].

predicting the two-phase inlet data with an MAE of 24.06% and showing an improvement compared to the single-phase inlet data. Shah's correlation for horizontal flow [36] produced an MAE of 27.14%, while the correlation for vertical upflow [34] has an MAE of 33.52%. The superiority of the horizontal correlation is due to the vertical upflow correlation now overpredicting q''_{CHF} for two-phase inlet. Similarly, the correlation of Tanaka *et al.* [81] experienced a decrease of 15% to an overall MAE for two-phase inlet of 34.21%. With a slight decrease in MAE to 34.77% the correlation of Zhang *et al.* [29] preformed relatively consistently. The accuracy of Basu *et al.*'s [84] correlation significantly improved for two-phase inlet conditions with an MAE of 36.59%. The correlations of Katto and Ohno [30], Zhang *et al.* [29], and Shah [34,36] are the only ones that consistently perform well for saturated CHF with both single-phase and two-phase inlet, with Shah's correlations excelling for subcooled CHF as well.

Most saturated CHF correlations showed mostly similar predictive accuracy for single-phase and two-phase inlets, but there are some notable deviations besides the ones already discussed. The correlations by Wu *et al.* [82] and Wu and Li [83] have MAEs that

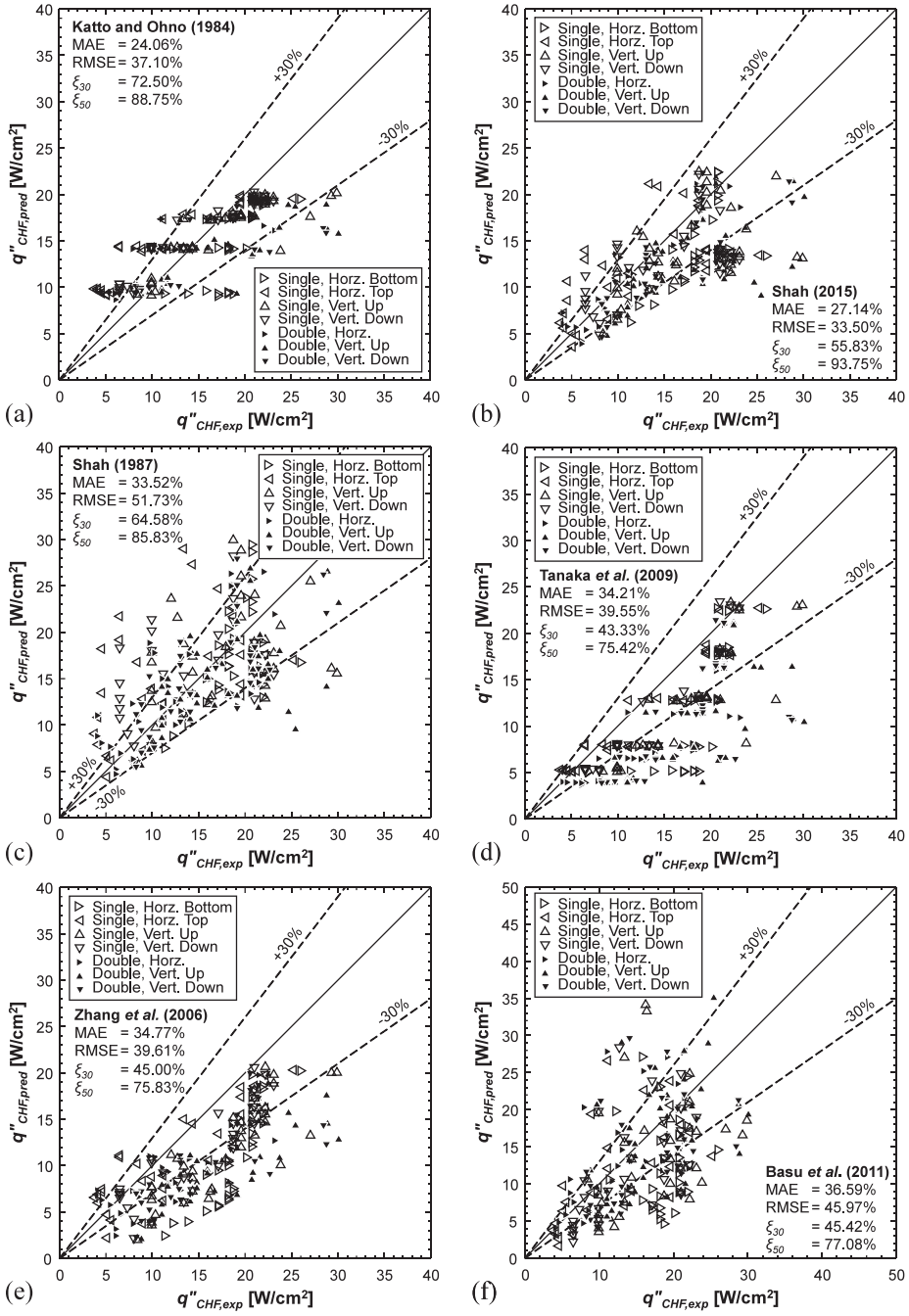

Fig. 7. Parity plots of the six best performing correlations for saturated CHF with two-phase inlet: (a) Katto and Ohno (1984) [30], (b) Shah (2015) [36], (c) Shah (1987) [34], (d) Tanaka *et al.* (2009) [81], (e) Zhang *et al.* (2006) [29], and (f) Basu *et al.* (2011) [84].

drastically increased when applied to two-phase inlet. These correlations are designed for cases with $BdRe^{0.5} \leq 200$. The present data greatly exceed this cut-off with a range of 586 – 3895 and the accuracy of predictions degrades at the higher outlet qualities experienced for two-phase inlet cases. Other correlations by Oh and Englert [88], Koşar *et al.* [87], and Ong and Thome [37], which performed poorly for single-phase inlet, also experienced a large increase in MAE of over 100% for two-phase inlet as compared to single-phase inlet. On the contrary, for two-phase inlet, the correlation by Green [86] showed significant improvement compared to its single-phase inlet predicitons. However, with an MAE of 138.98%, this correlation still proved unreliable.

4. Development of New CHF Correlation

4.1. Rationale and shortcomings of previous correlations

Even the most robust correlations such as those by Katto and Ohno [30] and Shah [34,36], which yielded good accuracies for large subsets of the FBCE-CHF database, lack the ability to predict the entire database with the former intended for saturated CHF, and the latter two unable to predict microgravity data. Other correlations are able to predict a small percentage of the database with good accuracy, such as, Tso *et al.* [71] and Shibahara *et al.* [67] for subcooled vertical upflow and Zhang *et al.* [29] for satu-

rated vertical downflow. However, the overall MAE of these correlations suffers from their inapplicability for other inlet qualities or orientations.

Most available flow boiling CHF correlations neglect the influence of gravity when predicting q''_{CHF}. This is a reasonable assumption for some correlations, particularly for those developed for either high inertia data, where flow inertia is dominant and CHF is independent of body force [48], or micro-channel data, where surface tension forces trump body forces [90]. However, outside of these conditions, body force plays a significant role and thus should not be absent in correlations aiming to accurately predict q''_{CHF}. Zhang *et al.* [40] showed the influence body force plays on CHF by investigating flow boiling in a channel at different orientations. They showed how the influence of gravity not only impacts q''_{CHF} but can change the physical mechanism that causes CHF.

A common remedy used to avoid the complexity of gravity's influence is to specify the orientation for which a correlation is applicable for, exacerbating the search for an appropriate correlation for one's geometry, heating configuration, operating conditions, and now, orientation. This also precludes using correlations for gravitational environments that are different from Earth's. Accounting for body force can be typically accomplished by utilizing a term that includes some combination of the Bond, Froude, or Confinement numbers. This can produce singularity as g approaches 0, which is experienced in space applications. Hence, there is a clear need for correlations that accurately capture the influence of gravity on q''_{CHF} while maintaining the robustness to account for classic influences such as inertia, subcooling, and pressure.

4.2. New correlation

The database presented in Table 1 is used to develop a simple, inlet conditions based, dimensionless, flow boiling CHF correlation that accounts for the impact of body force for a wide range of operating conditions encompassing both single-phase liquid and saturated two-phase inlets. The new correlation is developed with insights provided by the aforementioned correlations coupled with flow physics. These considerations ensure the new correlation will follow conventionally accepted trends shown in previous correlations, as well as avoid non-physical predictions. Non-linear regression, using a bisquare robust weighting function with a tuning constant of 4.685 [91], was performed in MATLAB software to determine the coefficients and verify the statistical significance of the functional form. Hypothesis testing considers two hypotheses: null and alternative. Null hypothesis assumes one parameter has no effect on another and is assumed true by default. Alternative hypothesis is the antithesis of the null hypothesis and states that one independent parameter has some effect on another. A p-value (probability value) gives the probability that the null hypothesis is true, and any given experiment will produce the value in the database. Null hypothesis is generally rejected when the p-value is less than 0.05 indicating the effect is statistically significant [12,92].

Starting with the dependence proposed by Hall and Mudawar [70], a non-dimensional correlation for CHF can be written as either

$$Bo_{CHF} = f\left(We, \frac{\rho_f}{\rho_g}, x_{e,in}, \frac{L_h}{D}\right) \tag{2}$$

or

$$Bo_{CHF} = f\left(We, \frac{\rho_f}{\rho_g}, x_{e,out}\right). \tag{3}$$

The former is selected in order to develop a correlation based on inlet conditions, which according to the authors, is more useful and easily applicable when making design predictions. CHF correlations typically define length as either L_h or L_{CHF}. An example of flow visualization at CHF [60] and temperature variations for a typical run resulting in CHF [62] taken from the MST dataset, albeit not the same run but runs with near identical operating conditions, are presented in Figs. 8(a) and 8(b), respectively. It is apparent in Fig. 8(a) that, at CHF, the heated wall is banketed by a vapor layer and the downstream region of the channel is primarily occupied by vapor. In Fig. 8(b), multiple downstream strip thermocouples are observed escalating to 122°C, indicating CHF and triggering a heater shut down. Thus, a specific location of CHF cannot be accurately determined. For simplicity and consistency, while ensuring satisfactory results, the channel's heated length is used in the development of the present correlation and is recommended in its application. Partial heating is accounted for by using a diameter based on the heated perimeter [52,53] of the channel when calculating dimensionless groups. Other methods of accounting for the heating configuration of the channel were considered, such as (i) Kureta and Akimoto's [56] dimensionless group of heated-to-wetted perimeter ratio, which when included, proved to be statistically insignificant, and (ii) modified diameters used by Cheng *et al.* [51] and Lee and Mudawar [54] directly in other dimensionless groups, which failed to enhance the correlation's predictive accuracy past the current method. One of the most apparent functional forms can be written as

$$Bo_{CHF} = C_1 We_{D_e}^{C_2}\left(\frac{L_h}{D_e}\right)^{C_3}\left(\frac{\rho_f}{\rho_g}\right)^{C_4}(1 - C_5 x_{e,in}). \tag{4}$$

Here, $(1\text{-}x_{e,in})$ is included to capture the physical trend of q''_{CHF} increasing as subcooling increases, resulting in a correlation with a similar form to that proposed by Katto and Ohno [30], where q''_{CHF} has a linear relationship with subcooling. Including observations by Hall and Mudawar [20,70], the constant within the subcooling term can be dependent on pressure. This is a simplification to Katto and Ohno's [30] correlation which also includes We and L_h/D. However, inclusion of these additional terms lessened the statistical significance of each term in the equation by increasing the calculated p-values during regression above the general cutoff. Including the new formulation of the subcooling term, the new functional form can be written as

$$Bo_{CHF} = C_1 We_{D_e}^{C_2}\left(\frac{L_h}{D_e}\right)^{C_3}\left(\frac{\rho_f}{\rho_g}\right)^{C_4}\left(1 - \left(\frac{\rho_f}{\rho_g}\right)^{C_5} x_{e,in}\right). \tag{5}$$

After non-linear regression, the resulting correlation yielded an MAE of 24.04%, providing only minor improvements over some exisiting correlations. However, the influence of gravity and orientation is still absent in the current formulation. In order to account for these effects, two additional terms, inspired by Zhang *et al.* [48], are included to capture key trends with respect to body force. First is the diminishing effect body force has on q''_{CHF} as inertia increases. Second is how the magnitude and direction of the acting body force impacts q''_{CHF}. Both of these are addressed in the nondimensional groups selected, considering the components of gravity acting parallel and perpendicular to the heated wall by replacing g with $g.sin\theta$ and $g.cos\theta$, respectively. Here θ is the angle of the heated wall with respect to the horizontal and $\theta = 0°$ corresponding to horizontal bottom-wall heating, as shown in Fig. 9. For double-sided heating, the angle of the wall leading to the minimum q''_{CHF} should be considered, where the opposite wall is calculated as $\theta_1 = 180° - \theta_2$. The influence of gravity parallel to the heated wall can be captured with the use of Froude number, Fr, which quantifies the ratio of inertia to body force. Replacing g with $g.sin\theta$ describes the relative magnitudes of inertia in the flow direction to body force that is parallel, or antiparallel, to the flow and heated wall. The component of gravity perpendicular to the

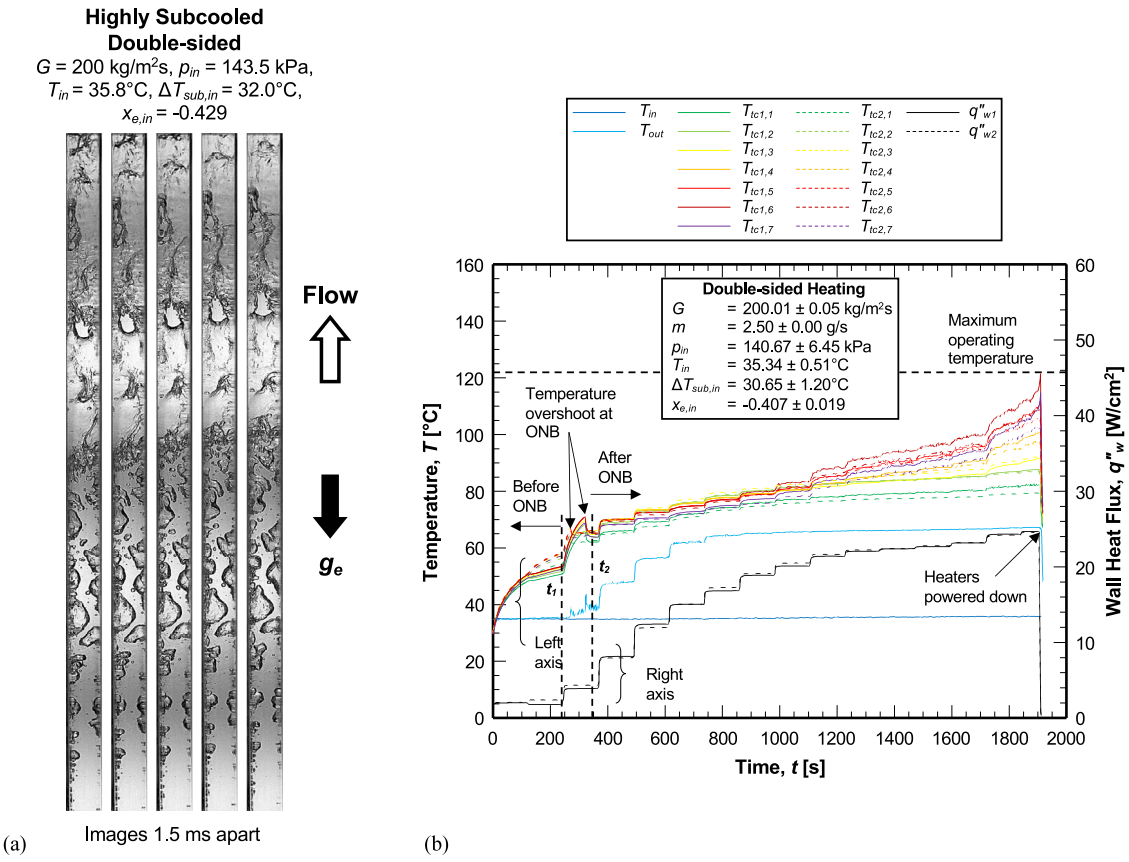

Fig. 8. (a) High-speed-video images of flow behavior at CHF (from [60]) and (b) temperature variation of fluid inlet, fluid outlet, and heater strip for heat flux increments from a minimum to CHF (from [62]).

wall is captured in the Bond number, *Bd*, replacing the *g* in *Bd* with *g.cosθ*. *Bd* quantifies the ratio of body force to surface tension forces which are prevalent as an interface develops along the heated wall during vapor production. As described by classical instability theory [93], surface tension and body force play key roles in determining the stability of an interface. During vapor production, this either aids in or inhibits vapor removal from the heated wall. Unlike *Fr*, *Bd* does not contain a term to account for the influence of inertia. *Bo* is divided by *We* to reflect the diminishing effect of body force as inertia becomes dominant. These terms are included in the final form for the correlation and can be written as

$$Bo_{CHF} = C_1 We_{D_e}^{C_2}\left(\frac{L_h}{D_e}\right)^{C_3}\left(\frac{\rho_f}{\rho_g}\right)^{C_4}\left(1-\left(\frac{\rho_f}{\rho_g}\right)^{C_5} x_{e,in}\right) \ldots\left(1+C_6\frac{1}{Fr_{\theta,D_e}}\right)\left(1+C_7\frac{Bd_{\theta,D_e}}{We_{D_e}^{C_8}}\right), \quad (6)$$

where orientation-specific Froude number is defined as

$$Fr_\theta = \frac{G^2}{\left(\rho_f^2 g \sin\theta D\right)} \quad (7)$$

and orientation-specific Bond number as

$$Bd_\theta = \frac{g\cos\theta\left(\rho_f-\rho_g\right)D^2}{\sigma}. \quad (8)$$

The terms containing *g* are composed in such a way that, as *g* approaches 0, the effect of gravity becomes absent, and physical trends are captured with respect to buoyancy's effect on a flow boiling system. As the inertia terms become relatively large, the influence of gravity is diminished. Non-linear regression is performed in MATLAB and it yields a p-value of 0.0103 for the leading coefficient, and the subsequent largest p-value is 2.03×10^{-10}, well below the general cutoff to reject the null hypothesis. A non-linear constrained minimization problem was then created in MATLAB to calculate the coefficients that minimize the MAE. Coefficients were constrained to avoid non-physical trends, and optimization resulted in the following final correlation,

$$Bo_{CHF} = 0.353 We_{D_e}^{-0.314}\left(\frac{L_h}{D_e}\right)^{-0.226}\left(\frac{\rho_f}{\rho_g}\right)^{-0.481}\left(1-\left(\frac{\rho_f}{\rho_g}\right)^{-0.094} x_{e,in}\right) \ldots\left(1+0.034\frac{1}{Fr_{\theta,D_e}}\right)\left(1+0.008\frac{Bd_{\theta,D_e}}{We_{D_e}^{0.543}}\right). \quad (9)$$

4.3. Comparison of correlation predictions with experimental data

Predictions are made using the new correlation for the entire database, and Table 8 shows the corresponding MAEs for different orientations/microgravity and subcoolings. Parity plots of q''_{CHF} predicted by the new correlation are shown in Fig. 10(a-c) for subcooled CHF, saturated CHF with single-phase inlet, and saturated CHF with two-phase inlet, respectively. The gross overall resulting MAE of the correlation for the entire database is found to be 17.44% with 86.57% and 96.64% of datapoints predicted within ±30% and ±50% errors, respectively. In general, the new correlation outperforms the vast majority of previous correlations, barring a few correlations that have exceptional performance for very specific operating conditions. The new correlation resulted in the lowest MAE for each subset of the database, subcooled CHF with subcooled inlet, 18.46%, saturated CHF with single-phase inlet, 20.66%, and sat-

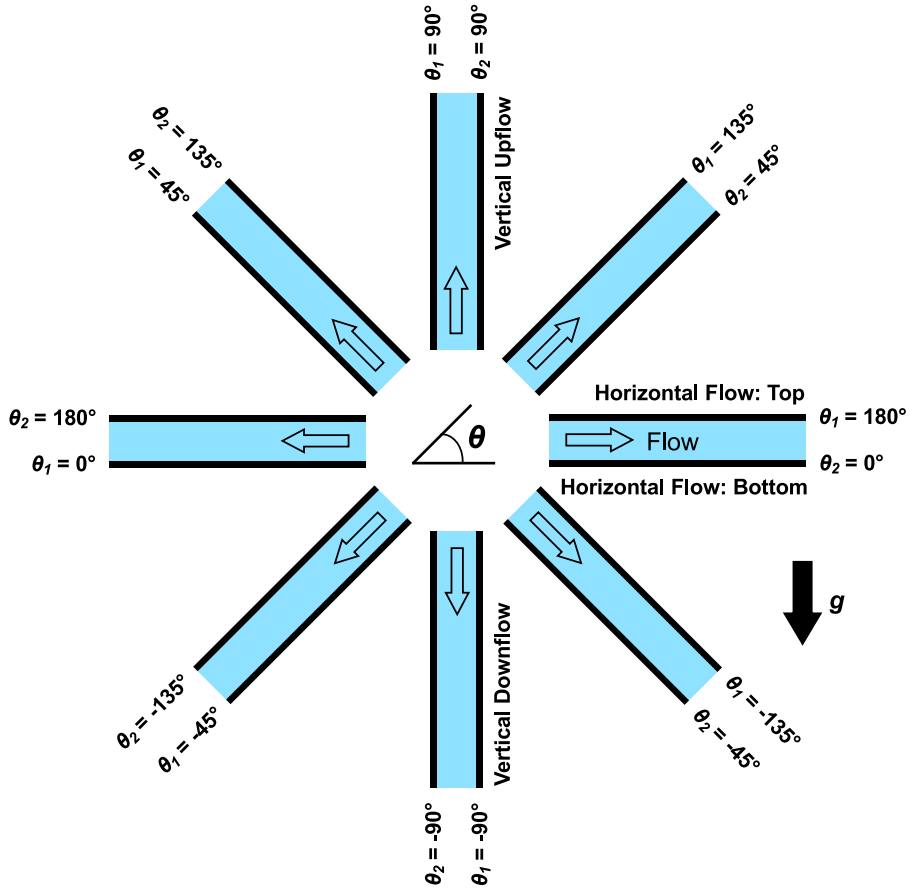

Fig. 9. Schematic of different flow orientations with respect to gravity and the corresponding wall angles.

Table 8
MAEs of the new correlation.

	Horizontal Flow				Vertical Upflow			Vertical Downflow			μg Flow			Overall
	Bottom	Top	Double	Overall	Single	Double	Overall	Single	Double	Overall	Single	Double	Overall	
Subcooled CHF	16.75	21.17	14.79	17.02	24.62	23.18	23.76	-	23.85	23.85	4.51	5.21	5.07	18.46
Saturated CHF with single-phase (liquid) inlet	21.80	12.15	25.01	20.87	25.42	19.34	21.43	39.87	29.58	31.29	12.76	18.07	16.80	20.66
Saturated CHF with two-phase inlet	8.54	18.88	22.70	16.95	15.41	13.51	14.41	15.28	15.95	15.62	-	-	-	15.76
Overall	13.25	18.30	20.74	17.79	18.41	16.42	17.28	16.04	19.08	17.85	9.74	17.40	14.84	17.44

urated CHF with two-phase inlet, 15.76%. The Root Mean Square Error, RMSE, defined as

$$RMSE(\%) = \sqrt{\frac{1}{N}\sum\left(\frac{q''_{CHF,pred} - q''_{CHF,exp}}{q''_{CHF,exp}}\right)^2} \times 100, \qquad (10)$$

gives higher weight to outliers, and shows a similar trend with the new correlation outperforming the existing correlations shown in Figs. 4, 5 and, 6 with respective RMSEs of 23.87%, 26.95%, and 22.59% for subcooled CHF with subcooled inlet, saturated CHF with single-phase inlet, and saturated CHF with two-phase inlet. The accuracy for the different subsets shows a significant benefit of the correlation in its consistancy across a wide variety of inlet qualities, ranging from subcooled liquid to two-phase mixture. For a given orientation, the largest variation in MAE between the three CHF types is 24.59%, which is observed between saturated CHF with subcooled inlet and saturated CHF with two-phase inlet for single-sided vertical downflow. The CHF predictions for the remainder of orientations fall within an MAE of 15% of each other. In the same manner, for a given CHF subset, the correlation predicts each orientation in Earth gravity, horizontal, vertical up, and vertical down, within an MAE of 11% of each other. This, coupled with the excellent predictions for microgavity data clearly indicate the correlation's capability to account for buoyancy.

Fig. 11 shows parametric trends of the new correlation compared to those of prior correlations and experimental results for various sets of operating conditions. Fig. 11(a) and (b) show predictions by the new and six-best-performing prior correlations for subcooled CHF [26,34,36,67–69] and saturated CHF with single-phase inlet [29,30,34,36,80,81], respectively, as $x_{e,in}$ is varied. Most correlations, including the new one, predict an almost linear trend of q''_{CHF} versus $x_{e,in}$. In Fig. 11(a), the new correlation shows good predictions for subcooled CHF in terms of both accuracy and trend. Prior correlations show similar trends excepting Celata *et al.* [26] which has a discontinuity at $x_{e,out}$ = -0.1. In Fig. 11(b), most correlations underpredict the trend and value of q''_{CHF}, including the new correlation with improved accuracy. The exception is the correlation by Tibiriça *et al.* [80] which overpredicts q''_{CHF}, with ex-

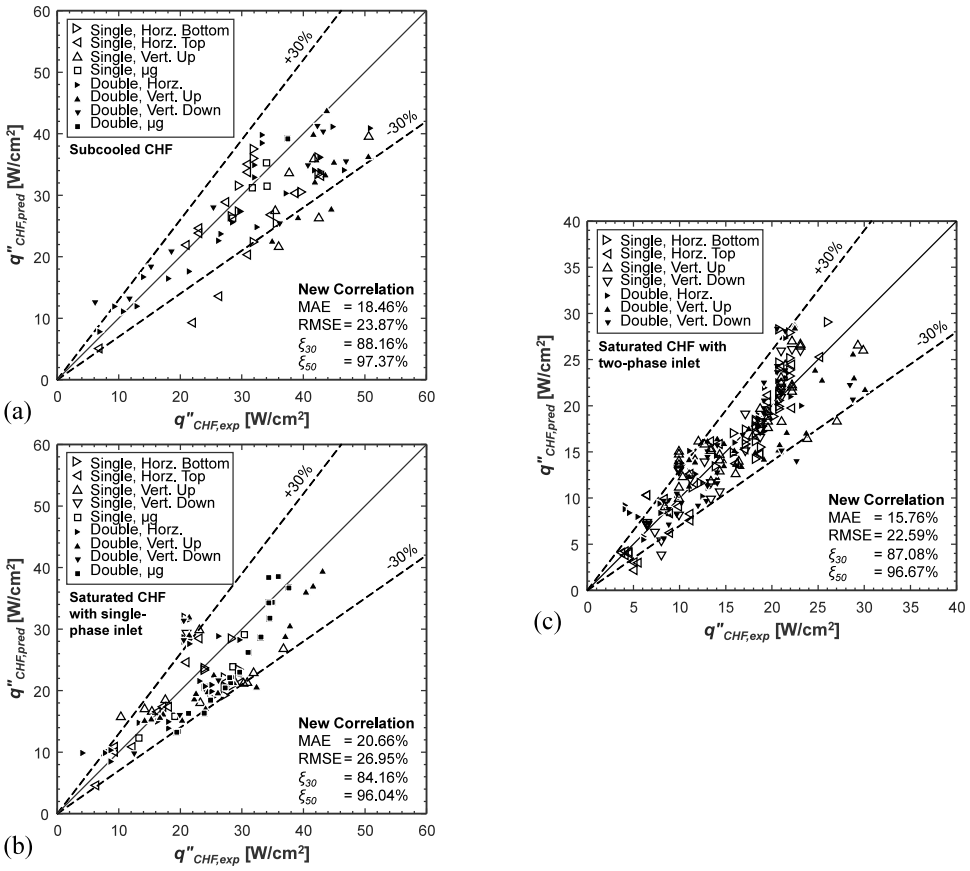

Fig. 10. Parity plots of the new CHF correlation for (a) subcooled CHF, (b) saturated CHF with single-phase (liquid) inlet, and (c) saturated CHF with two-phase inlet.

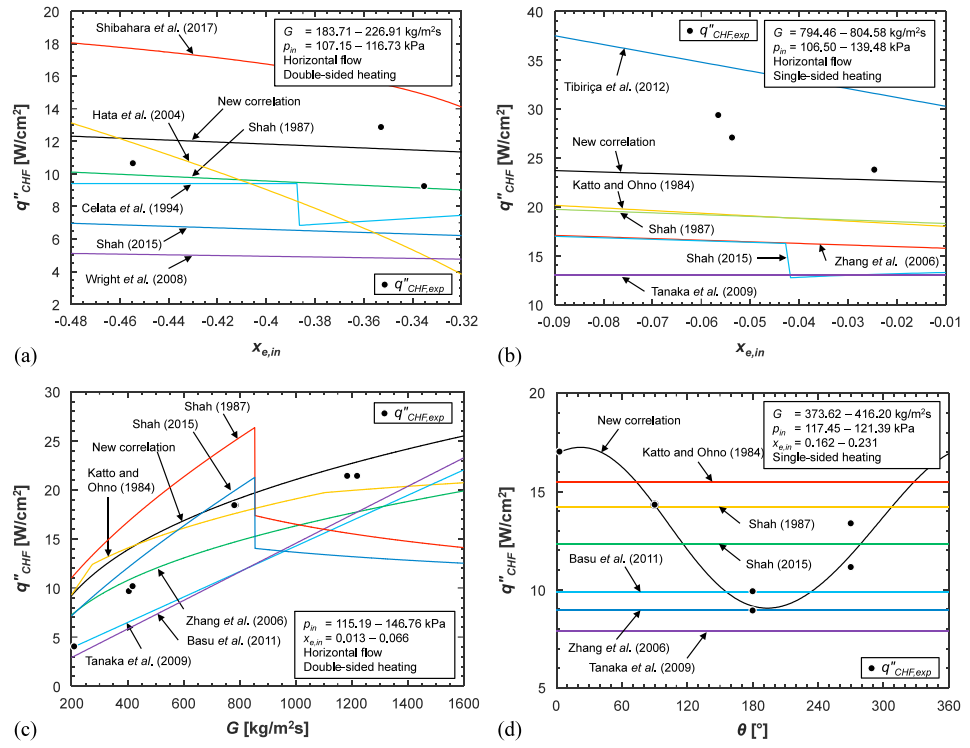

Fig. 11. Trends of new correlation compared to previous correlations with respect to (a) inlet quality for subcooled CHF, (b) inlet quality for saturated CHF, (c) mass velocity for two-phase inlet, and (d) orientation for two-phase inlet.

perimental results falling inbetween the predictions of their correlation and the new one. Fig. 11(c) shows CHF trends with respect to G for the six-best-performing CHF correlations for two-phase inlet [29,30,34,36,81,84]. The new correlation predicts a similar trend as Katto and Ohno's correlation [30] and follows the trend of experimental data. However, at low G, the experimental trends are closest to the predicitons by Zhang *et al.* [29]. The correlations by Shah for vertical upflow [34] and horizontal flow [36] show a discontinuity at transition between his different equations. Fig. 11(d) shows q''_{CHF} with respect to orientation for two-phase inlet and highlights the most prominent difference between the new and prior correlations. For a fixed set of operating conditions, existing correlations yield the same q''_{CHF} as channel orientation is varied. However, it is apparent that q''_{CHF} is greatly influenced by buoyancy and the new correlation captures buoyancy either promoting or inhibiting CHF.

4.4. Possible extrapolation to other operating conditions

The new correlation to capture gravitational effects on flow boiling CHF was developed from a database of and recommended for nPFH due to its potential for thermal management in space applications [63]. The current database is most limited in L/D and density ratio due to a singular geometry with two heating configurations and a relatively limited pressure range, as compared to water experiments where pressure spans orders of magnitude. However, the dimensionless form of the correlation implies applicability to other fluids, geometries, and operating conditions. The parameter ranges of the present database correspond to dimensionless group ranges of We_{De} = 15.24 – 19540.26, L_h/D_e = 5.73 – 11.46, ρ_f/ρ_g= 48.15 – 123.90, $x_{e,in}$ = -0.50 – 0.68, $1/Fr_{\theta,De}$ = -5.82 – 14.68, $Bd_{\theta,De}$ = -864.80 – 865.34, Bo = 0.0012 – 0.0285. The authors expect the correlation to be useable for other systems, given the inputs are within the dimesionless group ranges used to develop the present correlation, perhaps with some loss of accuracy.

For example, the consolidated database of Celata *et al.* [26] includes data from the experiments of Vandervort *et al.* [94] from which operating parameters are selected. Possible operating conditions for vertical upflow of water in a 1-mm diameter, 10-mm long, uniformly-heated tube heated tube are G = 10000 kg/m^{2}s, p_{in} = 1.5 MPa, and T_{in} = 50°C. This corresponds to We_{De} = 3031.3, L_h/D_e = 10.0, ρ_f/ρ_g= 114.1, $x_{e,in}$ = -0.34, $1/Fr_{\theta,De}$ = 5×10^{-5}, $Bd_{\theta,De}$ = 0 and Bo = 0.0021, which are all within the ranges of the new correlation. A physical prediction of q''_{CHF} = 41.1 MW/m^2 is obtained using the new correlation, which is within their reported range. Even with this promising preliminary result, caution should be used before extrapolating the correlation to other fluids or conditions outside of the recommended ranges prior to further validation.

5. Conclusions

This study consolidates previously-amassed CHF databases using the FBCE's FBM, which was launched to the ISS in August 2021 to collect crucial flow boiling CHF data in microgravity. This condolidated FBCE-CHF database encompasses a wide range of operating conditions (both subcooled liquid inlet of different inlet subcoolings and saturated two-phase inlet of different inlet qualities at different mass velocities, systems pressures), heating configurations (single- and double-sided inlet), and different gravitational environments (different orientations in Earth gravity, and microgravity). An exhaustive literature search was conducted to identify almost all flow boiling CHF correlations, which were categorized into three based on the type of CHF: subcooled CHF, saturated CHF with single-phase inlet, and saturated CHF with two-phase inlet. These prior correlations were used to make predictions of the FBCE-CHF database. A new, simple CHF correlation is proposed for the entire database and is applicable for the ranges of operating conditions listed in Table 1, which corresponds to We_{De} = 15.24 – 19540.26, L_h/D_e = 5.73 – 11.46, ρ_f/ρ_g= 48.15 – 123.90, $x_{e,in}$ = -0.50 – 0.68, $1/Fr_{\theta,De}$ = -5.82 – 14.68, $Bd_{\theta,De}$ = -864.80 – 865.34, Bo = 0.0012 – 0.0285. Caution should be exercised if extrapolating the present correlation outside of the recommended ranges. Key conclusions from this study are:

(1) Some correlations showed the ability to provide adequate q''_{CHF} predictions for large portions of the consolidated database, with some providing very good predictions for very specific operating conditions. The most notable correlations are those by Shah [34] and Katto and Ohno [30], both of which were validated for large databases, and proved effective for the conditions they were developed for.
(2) None of the existing correlations were capable of predicting the entire database with good accuracy due to inherent drawbacks stemming from both the flow physics assumptions made and the databases they were developed from. This was also due to the unique heating configurations and variety of gravitational effects captured in the FBCE-CHF database.
(3) The new CHF correlation was developed to have a single, simplistic dimensionless-group based correlation that could predict the entire database with good accuracy. This was made possible by including specific dimensionless groups that account for the different effects of gravity, including predictions for microgravity, a feature not seen in existing gravity-inclusive correlations. This new correlation proved capable of predicting the present database with an overall MAE of 17.44% and good accuracies for each subset of the database.

Declaration of Competing Interest

None declared.

Data Availability

The data that has been used is confidential.

Acknowledgement

The authors are grateful for the support of the National Aeronautics and Space Administration under grant no. 80NSSC22K0328. The authors thank their collaborators at NASA Glenn Research Center, especially Henry K. Nahra, R. Balasubramaniam, Mohammad M. Hasan, and Jeffrey R. Mackey. The authors also thank the entire FBCE team including Nancy Hall (FBCE Project Manager), Rochelle May and Phillip Gonia (Software Engineering), Mark Sorrells (Assembly, Integration and Test Lead), Jesse DeFiebre (Fluids Lead), Monica Guzik (FBCE Chief Engineer), and ZIN FCF Mission Operations Team for their dedicated technical support and the successful Mission Sequence Test.

References

[1] I. Mudawar, Two-phase microchannel heat sinks: theory, applications, and limitations, J. Electron. Packag. 133 (4) (2011) 041002, doi:10.1115/1.4005300.
[2] T.J. LaClair, I. Mudawar, Thermal transients in a capillary evaporator prior to the initiation of boiling, Int. J. Heat Mass Transfer 43 (21) (2000) 3937–3952, doi:10.1016/S0017-9310(00)00042-9.
[3] G. Liang, I. Mudawar, Review of pool boiling enhancement by surface modification, Int. J. Heat Mass Transfer 128 (2019) 892–933, doi:10.1016/j.ijheatmasstransfer.2018.09.026.
[4] I. Mudawar, R.A. Houpt, Mass and momentum transport in smooth falling liquid films laminarized at relatively high Reynolds numbers, Int. J. Heat Mass Transfer 36 (14) (1993) 3437–3448, doi:10.1016/0017-9310(93)90162-Y.
[5] C.O. Gersey, I. Mudawar, Effects of heater length and orientation on the trigger mechanism for near-saturated flow boiling critical heat flux—I. Photographic study and statistical characterization of the near-wall interfacial features, Int. J. Heat Mass Transfer 38 (4) (1995) 629–641, doi:10.1016/0017-9310(94)00193-Y.

[6] V.S. Devahdhanush, Y. Lei, Z. Chen, I. Mudawar, Assessing advantages and disadvantages of macro- and micro-channel flow boiling for high-heat-flux thermal management using computational and theoretical/empirical methods, Int. J. Heat Mass Transfer 169 (2021) 120787, doi:10.1016/j.ijheatmasstransfer.2020.120787.
[7] J. Lee, S.J. Darges, I. Mudawar, Experimental investigation and analysis of parametric trends of instability in two-phase micro-channel heat sinks, Int. J. Heat Mass Transfer 170 (2021) 120980, doi:10.1016/j.ijheatmasstransfer.2021.120980.
[8] S. Mukherjee, I. Mudawar, Pumpless loop for narrow channel and micro-channel boiling, J. Electron. Packag. 125 (3) (2003) 431–441, doi:10.1115/1.1602708.
[9] V.S. Devahdhanush, S. Lee, I. Mudawar, Experimental investigation of subcooled flow boiling in annuli with reference to thermal management of ultra-fast electric vehicle charging cables, Int. J. Heat Mass Transfer 172 (2021) 121176, doi:10.1016/j.ijheatmasstransfer.2021.121176.
[10] W.P. Klinzing, J.C. Rozzi, I. Mudawar, Film and transition boiling correlations for quenching of hot surfaces with water sprays, J. Heat Treat. 9 (2) (1992) 91–103, doi:10.1007/BF02833145.
[11] M.E. Johns, I. Mudawar, An ultra-high power two-phase jet-impingement avionic clamshell module, J. Electron. Packag. 118 (4) (1996) 264–270, doi:10.1115/1.2792162.
[12] V.S. Devahdhanush, I. Mudawar, Critical heat flux of confined round single jet and jet array impingement boiling, Int. J. Heat Mass Transfer 169 (2021) 12–14, doi:10.1016/j.ijheatmasstransfer.2020.120857.
[13] M.K. Sung, I. Mudawar, Correlation of critical heat flux in hybrid jet impingement/micro-channel cooling scheme, Int. J. Heat Mass Transfer 49 (15–16) (2006) 2663–2672, doi:10.1016/j.ijheatmasstransfer.2006.01.008.
[14] S.S. Kutateladze, A.I. Leont'ev, Some applications of the asymptotic theory of the turbulent boundary layer, in: Proc. Int. Heat Transfer Conf. 3, Begellhouse, Chicago, IL, USA, 1966, pp. 1–6, doi:10.1615/IHTC3.1920.
[15] J. Weisman, B.S. Pei, Prediction of critical heat flux in flow boiling at low qualities, Int. J. Heat Mass Transfer 26 (10) (1983) 1463–1477, doi:10.1016/S0017-9310(83)80047-7.
[16] C.H. Lee, I. Mudawwar, A mechanistic critical heat flux model for subcooled flow boiling based on local bulk flow conditions, Int. J. Multiphase Flow 14 (6) (1988) 711–728, doi:10.1016/0301-9322(88)90070-5.
[17] J.E. Galloway, I. Mudawar, CHF mechanism in flow boiling from a short heated wall—II. Theoretical CHF model, Int. J. Heat Mass Transfer 36 (10) (1993) 2527–2540, doi:10.1016/S0017-9310(05)80191-7.
[18] C.B. Tibiriçá, D.M. Rocha, I.L.S. Sueth, G. Bochio, G.K.K. Shimizu, M.C. Barbosa, S. dos S. Ferreira, A complete set of simple and optimized correlations for microchannel flow boiling and two-phase flow applications, Appl. Therm. Eng. 126 (2017) 774–795, doi:10.1016/j.applthermaleng.2017.07.161.
[19] D.D. Hall, I. Mudawar, Critical heat flux (CHF) for water flow in tubes-I. Compilation and assessment of world CHF data, Int. J. Heat Mass Transfer 43 (14) (2000) 2573–2604, doi:10.1016/S0017-9310(99)00191-X.
[20] D.D. Hall, I. Mudawar, Critical heat flux (CHF) for water flow in tubes-II. Subcooled CHF correlations, Int. J. Heat Mass Transfer 43 (14) (2000) 2605–2640, doi:10.1016/S0017-9310(99)00192-1.
[21] W.H. Jens, P.A. Lottes, Analysis of Heat Transfer, Burnout, Pressure Drop and Density Data for High-Pressure Water, Argonne National Laboratory, Argonne, IL, USA, 1951, doi:10.2172/4421630.
[22] R.A. DeBortoli, S.J. Green, B.W. LeTourneau, M. Troy, A. Weiss, Forced-Convection Heat Transfer Burnout Studies for Water in Rectangular Channels and Round Tubes at Pressures above 500 Psia, Westinghouse Electric Corp. Bettis Plant, Pittsburgh, PA, USA, 1958.
[23] W.R. Gambill, N.D. Greene, for Water in Vortex Flow, A Preliminary Study of Boiling Burnout Heat Fluxes, Oak Ridge National Laboratory, Oak Ridge, TN, USA, 1958, doi:10.2172/4306809.
[24] R.T. Jacobs, J.A. Merrill, The application of statistical methods of analysis for predicting burnout heat flux, Nucl. Sci. Eng. 8 (6) (1960) 480–496, doi:10.13182/NSE60-A25834.
[25] L.S. Tong, Prediction of departure from nucleate boiling for an axially non-uniform heat flux distribution, J. Nucl. Energy 21 (3) (1967) 241–248, doi:10.1016/S0022-3107(67)90054-8.
[26] G.P. Celata, M. Cumo, A. Mariani, Assessment of correlations and models for the prediction of CHF in water subcooled flow boiling, Int. J. Heat Mass Transfer 37 (2) (1994) 237–255, doi:10.1016/0017-9310(94)90096-5.
[27] L.S. Tong, Boundary-layer analysis of the flow boiling crisis, Int. J. Heat Mass Transfer 11 (7) (1968) 1208–1211, doi:10.1016/0017-9310(68)90037-9.
[28] C.L. Vandervort, A.E. Bergles, M.K. Jensen, An experimental study of critical heat flux in very high heat flux subcooled boiling, Int. J. Heat Mass Transfer 37 (Suppl. 1) (1994) 161–173, doi:10.1016/0017-9310(94)90019-1.
[29] W. Zhang, T. Hibiki, K. Mishima, Y. Mi, Correlation of critical heat flux for flow boiling of water in mini-channels, Int. J. Heat Mass Transfer 49 (5–6) (2006) 1058–1072, doi:10.1016/j.ijheatmasstransfer.2005.09.004.
[30] Y. Katto, H. Ohno, An improved version of the generalized correlation of critical heat flux for the forced convective boiling in uniformly heated vertical tubes, Int. J. Heat Mass Transfer 27 (9) (1984) 1641–1648, doi:10.1016/0017-9310(84)90276-X.
[31] Y. Katto, A generalized correlation of critical heat flux for the forced convection boiling in vertical uniformly heated round tubes, Int. J. Heat Mass Transfer 21 (12) (1978) 1527–1542, doi:10.1016/0017-9310(78)90009-1.
[32] Y. Katto, A generalized correlation of critical heat flux for the forced convection boiling in vertical uniformly heated round tubes—a supplementary report, Int. J. Heat Mass Transfer 22 (6) (1979) 783–794, doi:10.1016/0017-9310(79)90017-6.
[33] Y. Katto, An analysis of the effect of inlet subcooling on critical heat flux of forced convection boiling in vertical uniformly heated tubes, Int. J. Heat Mass Transfer 22 (11) (1979) 1567–1575, doi:10.1016/0017-9310(79)90136-4.
[34] M.M. Shah, Improved general correlation for critical heat flux during upflow in uniformly heated vertical tubes, Int. J. Fluid Fl. 8 (4) (1987) 326–335, doi:10.1016/0142-727X(87)90069-5.
[35] M.M. Shah, A generalized graphical method for predicting CHF in uniformly heated vertical tubes, Int. J. Heat Mass Transfer 22 (4) (1979) 557–568, doi:10.1016/0017-9310(79)90059-0.
[36] M.M. Shah, A general correlation for critical heat flux in horizontal channels, Int. J. Refrig. 59 (2015) 37–52, doi:10.1016/j.ijrefrig.2015.06.027.
[37] C.L. Ong, J.R. Thome, Macro-to-microchannel transition in two-phase flow: Part 2 – Flow boiling heat transfer and critical heat flux, Exp. Therm. Fluid Sci. 35 (6) (2011) 873–886, doi:10.1016/j.expthermflusci.2010.12.003.
[38] L. Wojtan, R. Revellin, J.R. Thome, Investigation of saturated critical heat flux in a single, uniformly heated microchannel, Exp. Therm. Fluid Sci. 30 (8) (2006) 765–774, doi:10.1016/j.expthermflusci.2006.03.006.
[39] F.P. Chiaramonte, J.A. Joshi, Workshop on Critical Issues in Microgravity Fluids, Transport, and Reaction Processes in Advanced Human Support Technology – Final Report, NASA TM-2004-212940, 2004 Washington, D.C., USA.
[40] H. Zhang, I. Mudawar, M.M. Hasan, Experimental and theoretical study of orientation effects on flow boiling CHF, Int. J. Heat Mass Transfer 45 (22) (2002) 4463–4477, doi:10.1016/S0017-9310(02)00152-7.
[41] C. Konishi, I. Mudawar, M.M. Hasan, Investigation of the influence of orientation on critical heat flux for flow boiling with two-phase inlet, Int. J. Heat Mass Transfer 61 (2013) 176–190, doi:10.1016/j.ijheatmasstransfer.2013.01.076.
[42] C.R. Kharangate, L.E. O'Neill, I. Mudawar, Effects of two-phase inlet quality, mass velocity, flow orientation, and heating perimeter on flow boiling in a rectangular channel: Part 2 – CHF experimental results and model, Int. J. Heat Mass Transfer 103 (2016) 1280–1296, doi:10.1016/j.ijheatmasstransfer.2016.05.059.
[43] M. Misawa, An experimental and analytical investigation of flow boiling heat transfer under microgravity conditions, University of Florida, Gainesville, FL, USA, 1993 Ph. D. thesis.
[44] B. Liu, B. Yuan, J. Zhou, J. Zhao, P. Di Marco, Y. Zhang, J. Wei, Y. Yang, Analysis of the critical heat flux of subcooled flow boiling in microgravity, Exp. Therm. Fluid Sci. 120 (2021) 110238, doi:10.1016/j.expthermflusci.2020.110238.
[45] H. Zhang, I. Mudawar, M.M. Hasan, Flow boiling CHF in microgravity, Int. J. Heat Mass Transfer 48 (15) (2005) 3107–3118, doi:10.1016/j.ijheatmasstransfer.2005.02.015.
[46] C. Konishi, H. Lee, I. Mudawar, M.M. Hasan, H.K. Nahra, N.R. Hall, J.D. Wagner, R.L. May, J.R. Mackey, Flow boiling in microgravity: Part 2 - Critical heat flux interfacial behavior, experimental data, and model, Int. J. Heat Mass Transfer 81 (2015) 721–736, doi:10.1016/j.ijheatmasstransfer.2014.10.052.
[47] C. Konishi, I. Mudawar, Review of flow boiling and critical heat flux in microgravity, Int. J. Heat Mass Transfer 80 (2015) 469–493, doi:10.1016/j.ijheatmasstransfer.2014.09.017.
[48] H. Zhang, I. Mudawar, M.M. Hasan, A method for assessing the importance of body force on flow boiling CHF, J. Heat Transfer 126 (2) (2004) 161–168, doi:10.1115/1.1651532.
[49] C. Konishi, I. Mudawar, M.M. Hasan, Criteria for negating the influence of gravity on flow boiling critical heat flux with two-phase inlet conditions, Int. J. Heat Mass Transfer 65 (2013) 203–218, doi:10.1016/j.ijheatmasstransfer.2013.05.070.
[50] L.E. O'Neill, I. Park, C.R. Kharangate, V.S. Devahdhanush, V. Ganesan, I. Mudawar, Assessment of body force effects in flow condensation, part II: Criteria for negating influence of gravity, Int. J. Heat Mass Transfer 106 (2017) 313–328, doi:10.1016/j.ijheatmasstransfer.2016.07.019.
[51] L. Cheng, G. Ribatski, J.M. Quibén, J.R. Thome, New prediction methods for CO2 evaporation inside tubes: Part I - A two-phase flow pattern map and a flow pattern based phenomenological model for two-phase flow frictional pressure drops, Int. J. Heat Mass Transfer 51 (1–2) (2008) 111–124, doi:10.1016/j.ijheatmasstransfer.2007.04.002.
[52] Y. Katto, General features of CHF of forced convection boiling in uniformly heated rectangular channels, Int. J. Heat Mass Transfer 24 (8) (1981) 1413–1419, doi:10.1016/0017-9310(81)90191-5.
[53] Z. Liu, R.H.S. Winterton, A general correlation for saturated and subcooled flow boiling in tubes and annuli, based on a nucleate pool boiling equation, Int. J. Heat Mass Transfer 34 (11) (1991) 2759–2766, doi:10.1016/0017-9310(91)90234-6.
[54] J. Lee, I. Mudawar, Critical heat flux for subcooled flow boiling in micro-channel heat sinks, Int. J. Heat Mass Transfer 52 (13–14) (2009) 3341–3352, doi:10.1016/j.ijheatmasstransfer.2008.12.019.
[55] R.K. Shah, A.L. London, Rectangular Ducts, Laminar Flow Forced Convection in Ducts (1978) 196–222, doi:10.1016/B978-0-12-020051-1.50012-7.
[56] M. Kureta, H. Akimoto, Critical heat flux correlation for subcooled boiling flow in narrow channels, Int. J. Heat Mass Transfer 45 (20) (2002) 4107–4115, doi:10.1016/S0017-9310(02)00129-1.
[57] C.R. Kharangate, L.E. O'Neill, I. Mudawar, M.M. Hasan, H.K. Nahra, R. Balasubramaniam, N.R. Hall, A.M. Macner, J.R. Mackey, Flow boiling and critical heat flux in horizontal channel with one-sided and double-sided heating, Int. J. Heat Mass Transfer 90 (2015) 323–338, doi:10.1016/j.ijheatmasstransfer.2015.06.073.
[58] C.R. Kharangate, L.E. O'Neill, I. Mudawar, M.M. Hasan, H.K. Nahra, R. Balasubramaniam, N.R. Hall, A.M. Macner, J.R. Mackey, Effects of subcooling and two-

phase inlet on flow boiling heat transfer and critical heat flux in a horizontal channel with one-sided and double-sided heating, Int. J. Heat Mass Transfer 91 (2015) 1187–1205, doi:10.1016/j.ijheatmasstransfer.2015.08.059.
[59] L.E. O'Neill, I. Mudawar, M.M. Hasan, H.K. Nahra, R. Balasubramaniam, N.R. Hall, A. Lokey, J.R. Mackey, Experimental investigation into the impact of density wave oscillations on flow boiling system dynamic behavior and stability, Int. J. Heat Mass Transfer 120 (2018) 144–166, doi:10.1016/j.ijheatmasstransfer.2017.12.011.
[60] S.J. Darges, V.S. Devahdhanush, I. Mudawar, H.K. Nahra, R. Balasubramaniam, M.M. Hasan, J.R. Mackey, Experimental results and interfacial lift-off model predictions of critical heat flux for flow boiling with subcooled inlet conditions – In preparation for experiments onboard the International Space Station, Int. J. Heat Mass Transfer 183 (2022) 122241, doi:10.1016/j.ijheatmasstransfer.2021.122241.
[61] V.S. Devahdhanush, S.J. Darges, I. Mudawar, H.K. Nahra, R. Balasubramaniam, M.M. Hasan, J.R. Mackey, Flow visualization, heat transfer, and critical heat flux of flow boiling in Earth gravity with saturated liquid-vapor mixture inlet conditions – In preparation for experiments onboard the International Space Station, Int. J. Heat Mass Transfer 192 (2022) 122890, doi:10.1016/j.ijheatmasstransfer.2022.122890.
[62] V.S. Devahdhanush, I. Mudawar, H.K. Nahra, R. Balasubramaniam, M.M. Hasan, J.R. Mackey, Experimental heat transfer results and flow visualization of vertical upflow boiling in Earth gravity with subcooled inlet conditions – In preparation for experiments onboard the International Space Station, Int. J. Heat Mass Transfer 188 (2022) 122603, doi:10.1016/j.ijheatmasstransfer.2022.122603.
[63] W.A. Arnold, T.G. Hartman, J. McQuillen, Chemical characterization and thermal stressing studies of perfluorohexane fluids for space-based applications, J. Spacecraft Rockets 44 (1) (2007) 94–102, doi:10.2514/1.22537.
[64] S. Lee, V.S. Devahdhanush, I. Mudawar, Experimental and analytical investigation of flow loop induced instabilities in micro-channel heat sinks, Int. J. Heat Mass Transfer 140 (2019) 303–330, doi:10.1016/j.ijheatmasstransfer.2019.05.077.
[65] E.W. Lemmon, I.H. Bell, M.L. Huber, M.O. McLinden, NIST Standard Reference Database 23: Reference Fluid Thermodynamic and Transport Properties-REFPROP, Version 10, NIST, 2018 Gaithersburg, MD, USA.
[66] C.L. Ong, J.R. Thome, Macro-to-microchannel transition in two-phase flow: Part 1 – Two-phase flow patterns and film thickness measurements, Exp. Therm. Fluid Sci. 35 (1) (2011) 37–47, doi:10.1016/j.expthermflusci.2010.08.004.
[67] M. Shibahara, K. Fukuda, Q.S. Liu, K. Hata, Correlation of high critical heat flux during flow boiling for water in a small tube at various subcooled conditions, Int. Commun. Heat Mass Transfer 82 (2017) 74–80, doi:10.1016/j.icheatmasstransfer.2017.02.012.
[68] K. Hata, M. Shiotsu, N. Noda, Critical heat fluxes of subcooled water flow boiling against outlet subcooling in short vertical tube, J. Heat Transfer 126 (3) (2004) 312–320, doi:10.1115/1.1725101.
[69] C.T. Wright, J.E. O'Brien, R.E. Spall, A new critical heat flux correlation for vertical water flow through multiple thin rectangular channels, Int. J. Heat Mass Transfer 51 (5–6) (2008) 1071–1084, doi:10.1016/j.ijheatmasstransfer.2007.05.013.
[70] D.D. Hall, I. Mudawar, Ultra-high critical heat flux (CHF) for subcooled water flow boiling-II: High-CHF database and design equations, Int. J. Heat Mass Transfer 42 (8) (1999) 1429–1456, doi:10.1016/S0017-9310(98)00242-7.
[71] C.P. Tso, K.W. Tou, G.P. Xu, Flow boiling critical heat flux of FC-72 from flush-mounted and protruded simulated chips in a vertical rectangular channel, Int. J. Multiphase Flow 26 (3) (2000) 351–365, doi:10.1016/S0301-9322(99)00023-3.
[72] I. Mudawar, D.E. Maddox, Critical heat flux in subcooled flow boiling of fluorocarbon liquid on a simulated electronic chip in a vertical rectangular channel, Int. J. Heat Mass Transfer 32 (2) (1989) 379–394, doi:10.1016/0017-9310(89)90184-1.
[73] K. Hata, M. Shiotsu, N. Noda, Critical heat flux of subcooled water flow boiling for high L/d region, Nucl. Sci. Eng. 154 (1) (2006) 94–109, doi:10.13182/NSE06-A2620.
[74] P.K. Sarma, V. Srinivas, K.V. Sharma, V.D. Rao, G.P. Celata, A correlation to evaluate critical heat flux in small diameter tubes under subcooled conditions of the coolant, Int. J. Heat Mass Transfer 49 (1–2) (2006) 42–51, doi:10.1016/j.ijheatmasstransfer.2004.07.052.
[75] V. Ganesan, R. Patel, J. Hartwig, I. Mudawar, Universal critical heat flux (CHF) correlations for cryogenic flow boiling in uniformly heated tubes, Int. J. Heat Mass Transfer 166 (2021) 120678, doi:10.1016/j.ijheatmasstransfer.2020.120678.
[76] P. Liu, Y. Guo, W. Ding, M. Tang, Y. Song, X. Peng, J. Ji, Q. Chen, X. Mao, Critical heat flux (CHF) correlations for subcooled water flow boiling at high pressure and high heat flux, J. Therm. Sci. 30 (1) (2021) 279–293, doi:10.1007/s11630-021-1394-7.
[77] A.P. Roday, M.K. Jensen, Study of the critical heat flux condition with water and R-123 during flow boiling in microtubes. Part II – Comparison of data with correlations and establishment of a new subcooled CHF correlation, Int. J. Heat Mass Transfer 52 (13–14) (2009) 3250–3256, doi:10.1016/j.ijheatmasstransfer.2009.02.004.
[78] K.M. Becker, D. Djursing, K. Lindberg, O. Eklind, C. Österdahl, Burnout Conditions for Round Tubes at Elevated Pressures, in: Proc. Int. Symp. Two-Phase Syst, Elsevier, 1972, pp. 55–73, doi:10.1016/B978-0-08-017035-0.50009-4.
[79] H. Nariai, F. Inasaka, Critical heat flux of subcooled flow boiling with water, with application to high heat flux components, Fusion Eng. Des. 9 (1989) 237–243, doi:10.1016/S0920-3796(89)80040-7.
[80] C.B. Tibiriçá, G. Ribatski, J.R. Thome, Saturated flow boiling heat transfer and critical heat flux in small horizontal flattened tubes, Int. J. Heat Mass Transfer 55 (25–26) (2012) 7873–7883, doi:10.1016/j.ijheatmasstransfer.2012.08.017.
[81] F. Tanaka, T. Hibiki, K. Mishima, Correlation for flow boiling critical heat flux in thin rectangular channels, J. Heat Transfer 131 (12) (2009) 1–7, doi:10.1115/1.3216037.
[82] Z. Wu, W. Li, S. Ye, Correlations for saturated critical heat flux in microchannels, Int. J. Heat Mass Transfer 54 (1–3) (2011) 379–389, doi:10.1016/j.ijheatmasstransfer.2010.09.033.
[83] Z. Wu, W. Li, A new predictive tool for saturated critical heat flux in micro/mini-channels: Effect of the heated length-to-diameter ratio, Int. J. Heat Mass Transfer 54 (13–14) (2011) 2880–2889, doi:10.1016/j.ijheatmasstransfer.2011.03.011.
[84] S. Basu, S. Ndao, G.J. Michna, Y. Peles, M.K. Jensen, Flow boiling of R134a in circular microtubes—part II: Study of critical heat flux condition, J. Heat Transfer 133 (5) (2011) 1–9, doi:10.1115/1.4003160.
[85] C. Martín-Callizo, R. Ali, B. Palm, Dryout incipience and critical heat flux in saturated flow boiling of refrigerants in a vertical uniformly heated microchannel, in: 6th Int. Conf. Nanochannels, Microchannels, Minichannels, ASMEDC, Darmstadt, Germany, 2008, pp. 705–712, doi:10.1115/ICNMM2008-62332.
[86] D. Mikielewicz, J. Wajs, M. Gliński, A.B.R.S. Zrooga, Experimental investigation of dryout of SES 36, R134a, R123 and ethanol in vertical small diameter tubes, Exp. Therm. Fluid Sci. 44 (2013) 556–564, doi:10.1016/j.expthermflusci.2012.08.018.
[87] A. Koşar, Y. Peles, A.E. Bergles, G.S. Cole, Experimental investigation of critical heat flux in microchannels for flow-field probes, in: 7th Int. Conf. Nanochannels, Microchannels Minichannels, ASMEDC, Pohang, South Korea, 2009, pp. 81–90, doi:10.1115/ICNMM2009-82214.
[88] C.H. Oh, S.B. Englert, Critical heat flux for low flow boiling in vertical uniformly heated thin rectangular channels, Int. J. Heat Mass Transfer 36 (2) (1993) 325–335, doi:10.1016/0017-9310(93)80008-I.
[89] W.J. Green, A flow boiling critical heat flux correlation for water and Freon-12 at low mass fluxes, Nucl. Eng. Des. 72 (3) (1982) 381–389, doi:10.1016/0029-5493(82)90051-6.
[90] W. Qu, S.M. Yoon, I. Mudawar, Two-phase flow and heat transfer in rectangular micro-channels, J. Electron. Packag. 126 (3) (2004) 288–300, doi:10.1115/1.1756589.
[91] P.W. Holland, R.E. Welsch, Robust regression using iteratively reweighted least-squares, Communications in Statistics - Theory and Methods 6 (9) (1977) 813–827, doi:10.1080/03610927708827533.
[92] H.J. Seltman, Experimental Design and Analysis, Department of Statistics, Carnegie Mellon University, 2018 https://www.stat.cmu.edu/~hseltman/309/Book/Book.pdf.
[93] H. Lamb, Hydrodynamics, 6th ed., Dover Publications, New York, NY, USA, 1945.
[94] C.L. Vandervort, A.E. Bergles, M.K. Jensen, The Ultimate Limits of Forced Convective Subcooled Boiling Heat Transfer, 1990 HTL 9, Troy, NY, USA.